Structural Engineering of Cathode Materials for Lithium–Sulfur Batteries

Ligui Li, Jingping Yu, Nan Wang, Jun Zhao, Bin Fan & Shuaibo Zeng

South China University of Technology, Guangzhou, China

&

Shaowei Chen

South China University of Technology, Guangzhou, China
University of California, Santa Cruz, CA, USA

1 INTRODUCTION

Lithium–sulfur (Li–S) batteries have been recognized as a promising energy technology to power stationary and portable electronic devices and electrical vehicles, since the discovery in the 1960s.[1] The typical reactions entail $Li \rightarrow Li^+ + e^-$ at the anode and $S + 2e^- \rightarrow S^{2-}$ at the cathode, with an overall reaction of $2Li + S \rightarrow Li_2S$.[2] Li–S batteries in general exhibit multiple merits. (i) Li–S batteries can deliver a theoretical energy density of 2567 Wh kg^{-1} that is nearly 10-fold higher than those of conventional Li-ion batteries (LIBs).[3,4] For instance, an energy density of about 180 Wh kg^{-1} is usually observed for $LiCoO_2$/C battery, 210 Wh kg^{-1} for $LiFePO_4$/C battery, 200 Wh kg^{-1} for $LiMnO_4$/C battery, and about 260 Wh kg^{-1} for $LiNi_{1/3}Mn_{1/3}Co_{1/3}$/C battery.[5,6] This is because of the high specific capacity of sulfur (1672 mAh g^{-1}), which can meet the ever-increasing demand of portable electronic devices and electrical vehicles.[7–9] (ii) Sulfur is one of the most abundant elements on the earth's crust, and more than 70 million tons of elemental sulfur are annually produced as a by-product from hydrodesulfurization in petroleum refining processes, coal desulfurization, etc.[10,11] (iii) Sulfur is a low-cost natural resource and readily accessible.[12,13] (iv) Sulfur is also environmentally compatible because of its low toxicity and low impacts to the environment.[9,14–16]

However, large-scale commercialization of the Li–S battery technology is greatly impeded by a series of challenging issues, which are mostly correlated with the cathode (Scheme 1). These include (i) poor electrical conductivity of sulfur and polysulfides ($\sim 5 \times 10^{-30}$ S cm^{-1} at 25 °C),[17–19] resulting in low specific capacity, low Coulombic efficiency, low utilization of active sulfur, and low charge–discharge rate performance; (ii) rapid mechanical degradation of cathode due to large volume expansion (up to 80%) of sulfur after complete lithiation; and (iii) dissolution of lithium polysulfides (Li_2S_x, $4 \leq x \leq 8$) into organic electrolytes and the subsequent so-called "shuttle" effects, which results in uncontrollable sulfide deposition on the anode of lithium metal, lowering the Coulombic efficiency, and causing rapid capacity attenuation.[20–23]

To mitigate these issues, a number of strategies have been developed and reported in recent literatures, mostly based on physical and/or chemical confinement of sulfur in a conductive matrix (Scheme 1). Therefore, in this article, we will summarize recent progress in the design and engineering of effective cathodes for Li–S battery that entails mostly physical and chemical confinements.

2 DESIGN AND ENGINEERING OF SULFUR CATHODES

2.1 Sulfur/Carbon Composites

In 1962, Herbert and Ulam were the first to demonstrate that sulfur might be used as a cathode material for lithium batteries.[1] Yet as the sulfur cathode exhibits only very low electrical conductivity,[24] sulfur is usually compounded with a conductive material. Among these, carbon materials are commonly used because of apparent electrical conductivity, high chemical stability, low density, and low costs. In early research, sulfur powders were simply mixed with toner in a physical manner, and the resulting cathodes usually showed only a poor electrochemical performance. Peled *et al.*[25] showed that by infilling sulfur into porous carbon, the specific capacity, and cycle stability of thus-prepared Li–S batteries could be markedly improved. An example for such a strategy was reported in 2009 by Ji *et al.*,[26] where sulfur was loaded into ordered mesoporous carbons, leading to significant enhancement of the cycling stability of the resulting Li–S cathode. A wider range of carbon materials of different morphologies have since been used as conductive supports in the preparation of S/C composites. These carbon materials also mitigate the issue of polysulfide dissolution into electrolyte by physical confinements and/or chemical adsorption. In addition, they minimize the negative impacts of poor electrical conductivity of sulfur and the large volume fluctuation during charge and discharge process because of the conductive carbon skeleton and porous structures.[27]

Encyclopedia of Inorganic and Bioinorganic Chemistry, Online © 2011–2019 John Wiley & Sons, Ltd.

This article was published in the *Encyclopedia of Inorganic and Bioinorganic Chemistry* in 2019 by John Wiley & Sons, Ltd.
DOI: 10.1002/9781119951438.eibc2687

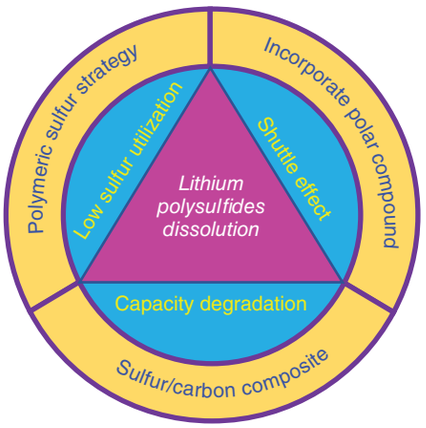

Scheme 1 Summary of the challenges that limit the performance of Li–S battery and mitigation strategies

2.1.1 Carbon Nanoparticles

Spherical or spheroidal carbon particles, due to their simple structure, small diameter, and large surface area, have been used rather extensively to effectively adsorb polysulfides through their surface functional groups. In fact, carbon particles have been widely utilized in the preparation of sulfur cathodes. In 2011, Archer and coworkers[28] utilized a simple silica hard-template method[29] to prepare mesoporous hollow carbon nanospheres. Experimentally, petroleum pitch was used as the carbon source, and after calcination at 1300 °C for 12 h under an argon flow, the silica templates were etched away by soaking in a HF solution, affording rather uniform hollow carbon nanospheres with a diameter of about 200 nm (Figure 1a). Molten sulfur was subsequently infiltrated into the hollow carbon nanospheres and used as the cathode for a Li–S battery, which retained a capacity of 850 mAh g^{-1} after 100 charge–discharge cycles at 0.5 C. It should be recognized, however, that although a considerable device performance can be achieved by using the hollow carbon nanospheres, the hard-template procedure involves several complicated, time-/energy-consuming processes, such as synthesis of nanospheres templates, homogeneous coating of precursor materials on the surface of nanosphere templates, and post-synthesis removal of the templates, which hinder scale-up production.

In another study, Xu *et al.*[30] proposed a "soft template" method without the physical templates and post-synthesis removal process. Experimentally, they used aniline and pyrrole as monomers and Triton X-100 as emulsifier to prepare uniform hollow carbon nanospheres with an ultra-high specific surface area over 3000 m^2 g^{-1} by low-temperature polymerization. The inner diameter of the obtained hollow carbon sphere was only about 70 nm (Figure 1b). By controlling the carbonization conditions, they found that the micropores on the surface of the hollow carbon nanospheres could be tailored but the hollow structure was preserved. After the loading of sulfur, the resulting S@C composite electrode showed a specific discharge capacity of 1240 mAh g^{-1} at 0.2 C. Note that although the encapsulation of sulfur in the mesopores hollow carbon nanospheres slowed down the dissolution of polysulfides, the weak interactions still allowed gradual diffusion of polysulfides out of these hollow carbon nanospheres during prolonged cycling. This suggests that physical confinement is not an effective strategy in achieving a stable performance of Li–S battery cathodes.

In 2013, Zhou *et al.*[31] prepared a sulfur-polyaniline composite and used it as the cathode material which exhibited excellent cycling stability. As shown in Figure 1(c), part of the hollow polyaniline nanospheres were loaded with sulfur, forming a unique yolk-shell structure. Because of the void space between the carbon shell and sulfur, volume expansion of sulfur during discharging was effectively alleviated. Using such a yolk-shell sulfur-polyaniline composite as the cathode material, the corresponding

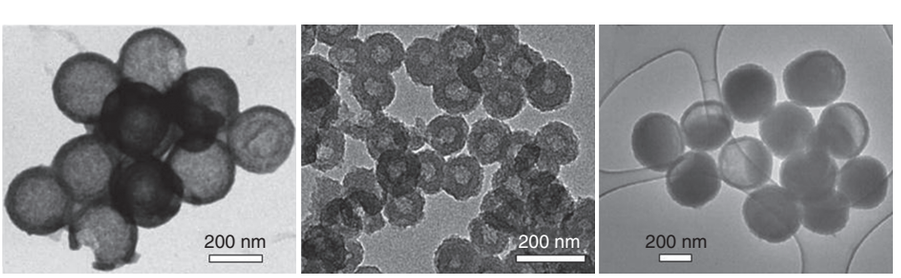

Figure 1 TEM images of hollow carbon nanospheres prepared by the (a) hard template method; (b) soft template method. (c) TEM images for yolk-shell carbon nanospheres. [Panel (a) reproduced with permission from Ref. 28. © Wiley-VCH Verlag GmbH & Co. KGaA; panel (b) reproduced with permission from Ref. 30. © 2015, Nature Publishing Group; panel (c) reprinted with permission from Ref. 31. © 2013, American Chemical Society]

Encyclopedia of Inorganic and Bioinorganic Chemistry, Online © 2011–2019 John Wiley & Sons, Ltd.

This article was published in the *Encyclopedia of Inorganic and Bioinorganic Chemistry* in 2019 by John Wiley & Sons, Ltd.
DOI: 10.1002/9781119951438.eibc2687

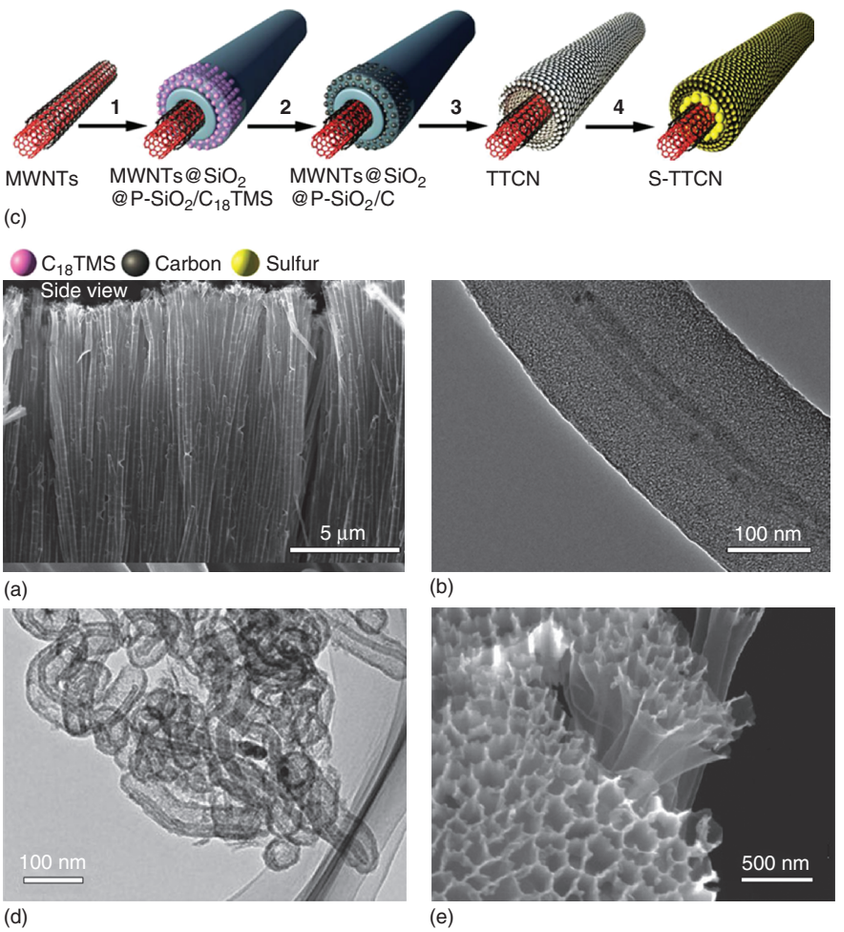

Figure 2 SEM image of (a) disordered carbon nanotubes prepared by template-wetting method; (b) TEM image of microporous carbon layer-coated carbon nanotube; (c) schematic of the synthesis of tube-in-tube structured carbon nanomaterial; (d) TEM image of tube-in-tube structured carbon nanomaterials; (e) SEM image of hollow carbon nanofiber array. [Panel (a) was reprinted with permission from Ref. 38. © 2011, American Chemical Society; panel (b) was reprinted with permission from Ref. 39. © 2012, American Chemical Society; and panel (c) was reproduced with permission from Ref. 36. © 2014, Wiley-VCH Verlag GmbH & Co. KGaA; panels (d,e) were reprinted with permission from Ref. 40. © 2011, American Chemical Society]

Li–S battery displayed a capacity of 765 mAh g^{-1} at 0.2 C and retained a specific capacity of 628 mAh g^{-1} after 200 charge–discharge cycles at 0.5 C.

2.1.2 Carbon Nanotubes

Carbon nanotubes (CNTs) are another structural scaffolds used extensively for sulfur cathodes in Li–S battery, because the hybridization orbitals of the π electrons are perpendicular to the plane of the carbon atoms, leading to excellent electrical conductivity along the tubular axis.[32,33] Carbon fibers have also been utilized widely because of their excellent mechanical properties, chemical stability, and electrical and thermal conductivity.[34,35] However, the main issue of these one-dimensional carbon structures is their low porosity and hence low specific surface area (typically less than 200 m^2 g^{-1}), which renders them ineffective in preventing the dissolution and diffusion of lithium polysulfides.[36,37]

To solve these problems, Wang and coworkers[38] developed a template wetting technique to prepare disordered carbon nanotubes (DCNTs). They used commercial anodic aluminum oxide (AAO) membranes as templates, into which sulfur was filled by physical vapor deposition (PVD). As shown in Figure 2(a), the vaporized sulfur diffused into the tiny voids of the graphitized carbon layers and defects in amorphous carbon. Thermal treatment of the sulfur powders at high temperatures led to the decomposition of S_8 molecules into smaller S_6 or S_2. These small molecules are able to pass through tiny pores in the shell and form more stable S_8 macromolecules. Note that these tiny channels can also effectively impede

Encyclopedia of Inorganic and Bioinorganic Chemistry, Online © 2011–2019 John Wiley & Sons, Ltd.

This article was published in the *Encyclopedia of Inorganic and Bioinorganic Chemistry* in 2019 by John Wiley & Sons, Ltd.
DOI: 10.1002/9781119951438.eibc2687

the penetration of liquid electrolyte and avoid the dissolution of polysulfides. The cathode material based on such sulfur-impregnated DCNTs exhibited excellent cycle stability and an unprecedented high Coulombic efficiency of 96% in 2011. Subsequently, Xin *et al.*[39] deposited a ~100 nm thick microporous carbon layer onto multiwalled carbon nanotubes (MWCNTs) to synthesize carbon nanotubes@microporous carbon (CNT@MPC) structures which were then heat-treated with the long-chain S_8 for a long time (155 °C, 20 h) to form short-chain $S_{2–4}$ allotropes, as shown in Figure 2(b). These metastable small $S_{2–4}$ molecules were confined within the MPC layers with a pore size of about 0.5 nm, which avoided the unfavorable transition from S_4^{2-} to S_8 during charge and discharge and fundamentally solved the problem of dissolution and diffusion of polysulfides in Li–S batteries. A Li–S battery prepared with this material exhibited excellent cycle stability and rate performance, and the first discharge specific capacity at 0.1 C reached 1670 mAh g^{-1}, very close to the theoretical capacity of sulfur (1675 mAh g^{-1}). The capacity was 800 mAh g^{-1} at 5 C, and after 200 cycle at 0.1 C, it still reached 1149 mAh g^{-1}. However, the sulfur loading remained too low. If too much sulfur was loaded into the hybrid carbon, the utilization rate would be reduced. In response to this situation, Xu and coworkers[36] reported a novel tube-in-tube carbon nanomaterial, as shown in Figure 2(c). They first treated the CNTs with acid and then coated the treated nanotubes with SiO_2 using an organosilicon compound (octadecyltrichlorosilane, C_{18}TMS) as the porogen agent and carbon precursors. After high-temperature calcination, C_{18}TMS was converted into carbon, and then SiO_2 was etched away with a NaOH solution to obtain a tube-in-tube carbon nanomaterial. Sulfur was then infiltrated into the gap between the tubes and into the tube by melt infiltration. This unique tube-in-tube structure not only improves the electrical conductivity of the CNTs but also increases the sulfur loading. As a cathode material for lithium–sulfur batteries, it exhibits an excellent electrochemical performance. At the current density of 500 mA g^{-1}, the discharge specific capacity still reached 918 mAh g^{-1} after 500 cycles.

In addition to CNTs, carbon fibers have also been widely used in Li–S batteries. Cui and coworkers[40] used an AAO film as a template to obtain a hollow carbon nanofiber array by carbonization of polystyrene, as shown in Figure 2(d) and (e). The AAO film was not only a template for the formation of carbon nanofibers but also prevented sulfur from depositing on the outer surface of the carbon fiber, thereby facilitating the penetration of sulfur into the interior of the carbon nanofiber. The hollow structure of carbon fibers effectively alleviated volume change of sulfur during charging and discharging. Owing to the thin carbon walls and large voids, lithium ions can penetrate easily. This hollow carbon fiber array can not only enable facile transport of electrons but also provide a large deposition area for Li_2S_2 and Li_2S. In fact, Li–S battery based on this material exhibited excellent electrochemical performance, with a high specific capacity of about 730 mAh g^{-1} at 0.2 C rate after 150 cycles of charge/discharge. Further introduction of $LiNO_3$ additive into the electrolyte was proven to improve the Coulombic efficiency to over 99% at 0.2 C.

2.1.3 *Graphene Derivatives*

Two-dimensional carbon nanomaterials have also been employed in the design and fabrication of sulfur cathode, such as graphene.[41,42] However, simple physical mixing of graphene and sulfur does not form an effective constraint on sulfur. During the charge and discharge processes, polysulfides can easily diffuse out of the sheet structure of graphene, compromising the battery performance. Cui and coworkers[43] developed a graphene–sulfur composite by coating sulfur particles with a surfactant and loading them onto carbon black-decorated graphene oxide (GO) sheets (Figure 3a–c). The graphene layer conducted electricity and confined the polysulfide intermediates, and the active agent layer accommodated volume change of sulfur during charging and discharging. This graphene–sulfur composite material exhibited an excellent electrochemical performance as a cathode material for Li–S batteries. The capacity was stable at 600 mAh g^{-1} at 0.2 C and decayed only 15% after 100 cycles. In another study, Zhang *et al.*[44] synthesized graphene oxide sheets using the modified Hummers method, and then nitridized the graphene oxide (GO) sheets under an NH_3 atmosphere to obtain nitrogen-doped graphene (NG). Ultrafine sulfur particles were then deposited on the NG sheets by chemical reduction. A Li–S battery with this S@NG material as the positive electrode showed a specific discharge capacity of 1167 mAh g^{-1} at 0.2 C, and the capacity decayed only 0.028% per cycle in 2000 cycles at 2 C. In a separate study, Yang and coworkers[45] recycled industrial waste gas H_2S to prepare high-performance electrode materials for Li–S battery, whereby they reduced graphene oxide (rGO) with H_2S to obtain a graphene/sulfur composite. The sulfur particles were uniformly dispersed on the graphene sheets, which were interconnected with a crimped structure.

It is well-known that graphene sheets are prone to stacking because of strong π–π interaction. This will compromise the specific surface area and seriously affect the energy storage property. A number of strategies have been reported to inhibit the stacking of graphene. For instance, Zhao *et al.*[46] synthesized unstacked bilayer graphene by template-directed chemical vapor deposition. They used mesoporous SiC nanosheets as a template to deposit graphene and form graphene protrusions at the mesopores. These protrusions acted as a barrier to prevent stacking of graphene layers on both sides of the nanosheets, as shown in Figure 3(d)–(e). The graphene synthesized by

Encyclopedia of Inorganic and Bioinorganic Chemistry, Online © 2011–2019 John Wiley & Sons, Ltd.

This article was published in the *Encyclopedia of Inorganic and Bioinorganic Chemistry* in 2019 by John Wiley & Sons, Ltd.
DOI: 10.1002/9781119951438.eibc2687

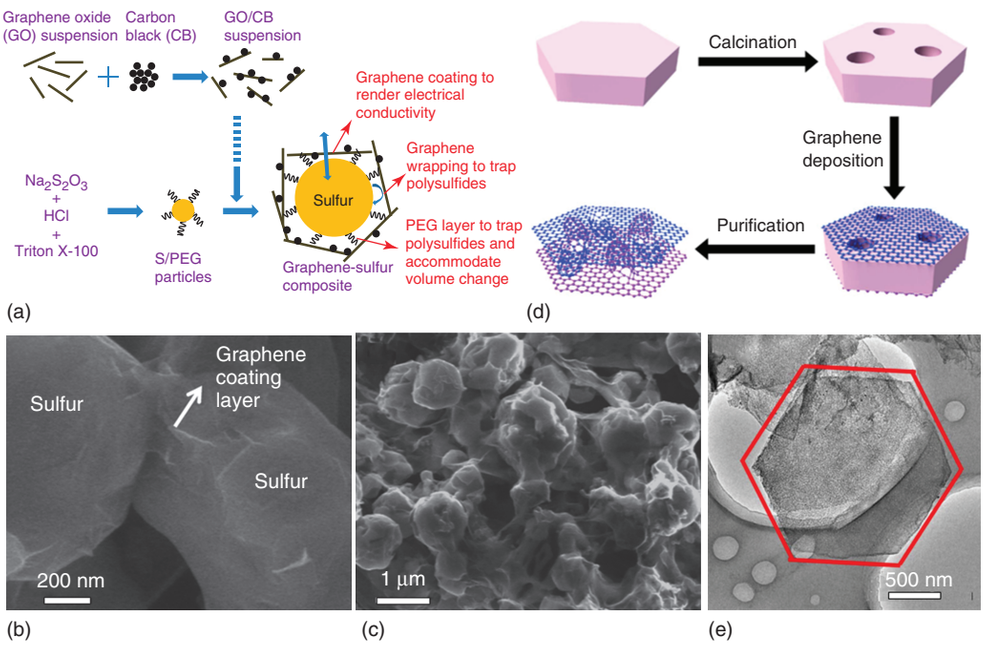

Figure 3 (a) Schematic of the synthesis of a graphene–sulfur composite. (b,c) Representative SEM images of the graphene–sulfur composite. (d) Unstacked two-layer graphene synthesis scheme. (e) TEM image of unstacked two-layer graphene. [Panels (a–c) were reprinted with permission from Ref. 43. © 2011, American Chemical Society; panels (d,e) were reproduced with permission from Ref. 46. © 2014, Nature Publishing Group]

this method showed high electrical conductivity; and loading of sulfur into the mesoporous structure effectively adsorbed polysulfides, inhibited the shuttle effect, and thus exhibited an excellent electrochemical performance. The specific discharge capacity reached 1034 and 734 mAh g^{-1} at the high rates of 5 and 10 C, respectively. After 1000 cycles at 5 C, the specific discharge capacity still reached 530 mAh g^{-1}.

The Li–S batteries described above generally use an aluminum foil as a current collector, which accounts for 5–9% of the total weight of the battery, and thereby reduces the energy density of the battery.[47] Cheng and coworkers[48] proposed a unique sandwich structure (Figure 4), where they used graphene as the cathode current collector and membrane, forming a unique graphene–sulfur–graphene-separator structure between the cathode active material and the separator. The graphene layer was used as a protective layer, conductive layer, and also separator for the battery, which suppressed the shuttle effects of lithium polysulfides. The use of graphene as a positive current collector not only simplifies the electrode preparation process but also increases the energy density of the battery.

2.1.4 Three-Dimensional Carbon Scaffolds

Three-dimensional (3D) carbon scaffolds, consisting of a network of carbon nanoparticles and graphene, generally show a high specific surface area and a rich pore structure that can facilitate electron and ion transport.[49] Such a structure is also advantageous to increase sulfur loading, which is typically low with carbon nanoparticles or graphene alone. For instance, Zheng and coworkers[50] prepared hierarchical porous carbon rods (HPCR) decorated with vertically oriented porous graphene-like nanosheets. As depicted in Figure 5(a), MgO microrods were first hydrolyzed at room temperature to produce $Mg(OH)_2$ microrods decorated with vertically oriented $Mg(OH)_2$ nanosheets. Graphene-like carbon layers were then grown by chemical vapor deposition onto these $Mg(OH)_2$ microrods in a CH_4 atmosphere. After the removal of MgO by etching with a HCl aqueous solution, a carbon rod composed of vertically aligned porous carbon sheets was obtained (Figure 5b). The obtained 3D porous carbon showed a high specific surface area of 2226 cm^2 g^{-1} and pore volume of 4.9 cm^3 g^{-1}. The skeleton consisted of interconnected vertical porous carbon sheets, a unique feature favorable for ion and electron transport. A Li–S battery with this material as the positive sulfur carrier exhibited an excellent electrochemical performance, and the reversible capacity reached 700 mAh g^{-1} after 300 cycles at 1 C.

In another study, Hoffmann *et al.*[51] used silica nanospheres as templates and immersed them in a polycarbosilane precursor to obtain a SiC/SiO_2 composite. After removal of the silica template, a porous carbon

Encyclopedia of Inorganic and Bioinorganic Chemistry, Online © 2011–2019 John Wiley & Sons, Ltd.

This article was published in the *Encyclopedia of Inorganic and Bioinorganic Chemistry* in 2019 by John Wiley & Sons, Ltd.
DOI: 10.1002/9781119951438.eibc2687

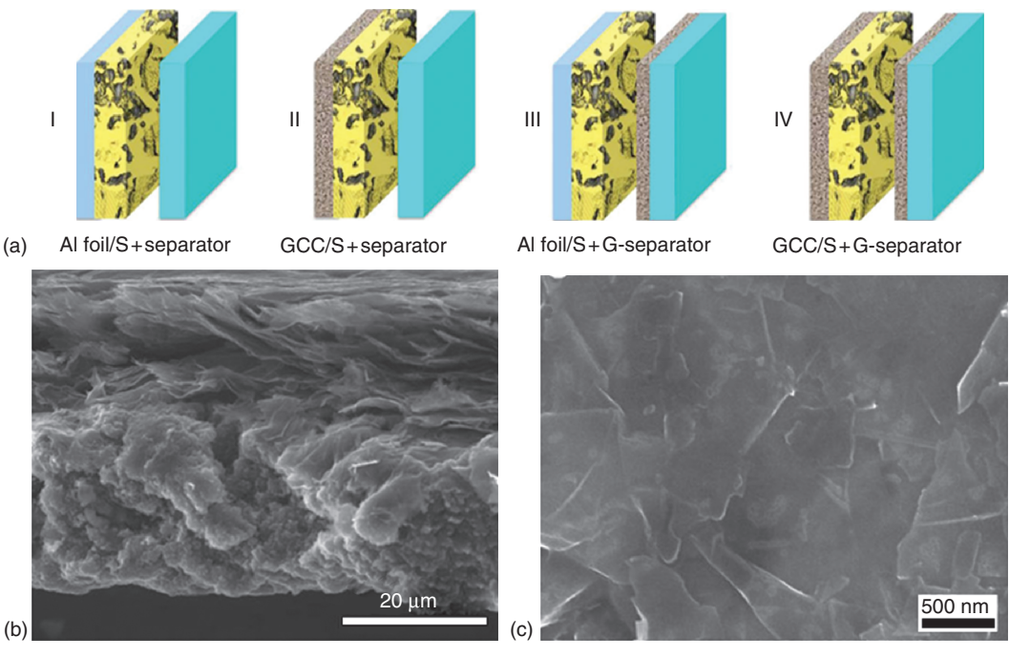

Figure 4 (a) Diagram of an electrode structure formed by different materials. (b) SEM image of a graphene–sulfur–graphene sandwich structure. (c) SEM image of graphene nanosheets on a graphene separator. [Reproduced with permission from Ref. 48, © 2014, Wiley-VCH Verlag GmbH & Co. KGaA]

material having monodisperse pores, pore size-adjustable and microporous carbon wall was obtained, as shown in Figure 5(c) and (d). This material showed an extremely high specific surface area of 2450 $m^2 g^{-1}$ and pore volume of 5 $cm^3 g^{-1}$. The large pores provided a high sulfur loading of 80 wt%, and the first specific discharge capacity of the battery with this material as the positive electrode reached 1165 mAh g^{-1} at 0.1 C. In a separate study, Yuan *et al.*[52] prepared carbon nanopaper with a 3D interconnected conductive frame. CNTs of different lengths were alternately connected in the carbon paper. Short CNTs were employed as the short-range electrical conductive framework for sulfur accommodation, while long CNTs formed the basis of conductive networks and mechanical scaffolds. Such a material exhibited a sulfur loading of 17.3 mg cm^{-2} and an area capacity of 15.1 mAh cm^{-2}.

In the above studies, the electrochemical performance of the sulfur/carbon composite electrodes was improved due to an increase of the specific surface area and pore volume of the electrode, but the influence of the structural characteristics on the electron-transfer kinetics was inadequately explained. Huang and coworkers[53] pointed out that smaller sulfur molecules have better cycle stability and electrolyte compatibility, but their discharge voltage platform is too low, thus reducing the energy density of the battery. Although larger sulfur molecules have a higher discharge platform, they can only exist in larger pores, and the electrolyte solution can easily penetrate into these large pores and cause dissolution and diffusion of polysulfides. If the advantages of the smaller sulfur molecules of S_{2-4} and the larger S_8 molecule can be combined, it is possible to further improve the electrochemical performance of the battery. This will necessitate the development of new effective strategies in electrode design and engineering.

2.2 Polymeric Sulfur Strategy

The strategies described in the earlier section are primarily focused on physical methods to suppress polysulfide dissolution and the shuttle effects. The corresponding batteries often suffer a rapid decrease of capacity during charge–discharge cycles and hence have limited applications. Note that at ambient conditions, elemental sulfur exists in the form of an eight-membered ring (S_8). When elemental sulfur is heated up to 159 °C, equilibrium ring-opening polymerization (ROP) can start and form linear polysulfane with diradical chain ends. Chemical copolymerization strategies can, therefore, be employed to avoid the dissolution of long-chain polysulfides by copolymerization with different organic monomers, forming strong covalent bonds between the carbon frameworks and sulfur. Herein, we highlight three copolymers that have been used in Li–S batteries.

Encyclopedia of Inorganic and Bioinorganic Chemistry, Online © 2011–2019 John Wiley & Sons, Ltd.

This article was published in the *Encyclopedia of Inorganic and Bioinorganic Chemistry* in 2019 by John Wiley & Sons, Ltd.
DOI: 10.1002/9781119951438.eibc2687

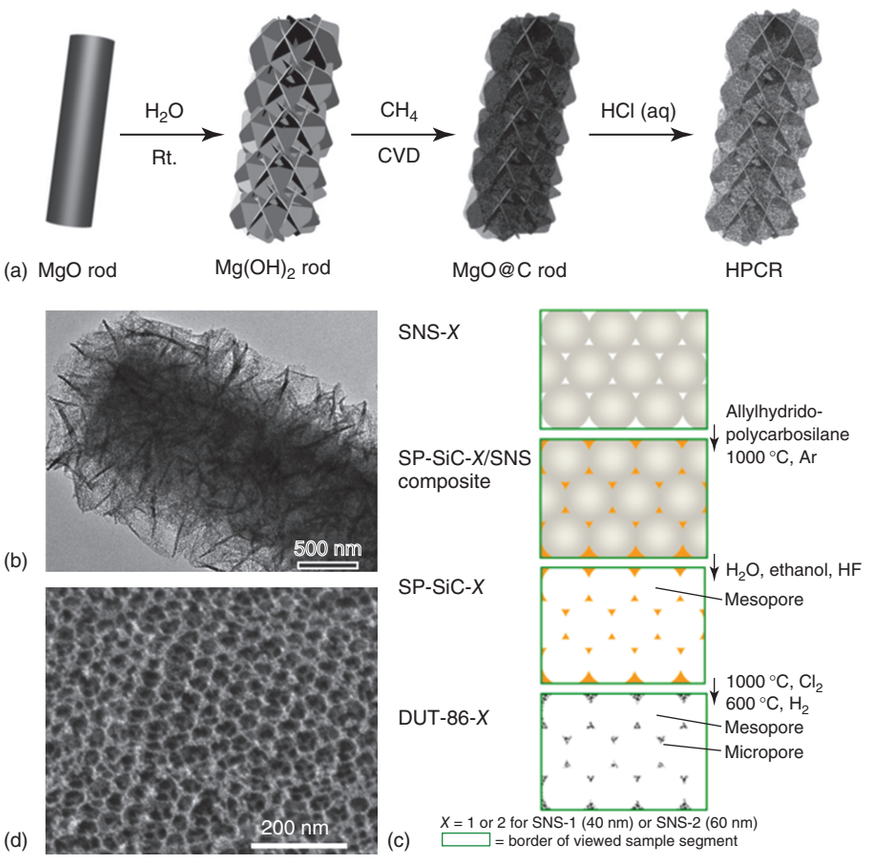

Figure 5 (a) Schematic of the synthetic process for HPCR. (b) TEM image of HPCR. (c) Synthesis scheme from parent silica nanospheres (SNS-*X*) to nanoporous silicon carbides (SP-SiC-*X*) and further to carbide-derived carbon materials (DUT-86-*X*) with $X = 1$ and 2 for silica sphere size of 40 and 60 nm, respectively. White parts symbolize pores. (d) SEM image of microporous carbon wall porous carbon material. [Panels (a,b) were reproduced with permission from Ref. 50, © 2016, Wiley-VCH Verlag GmbH & Co. KGaA; panels (c,d) were reprinted with permission from Ref. 51. © 2014, American Chemical Society]

2.2.1 Alkene-Derived Organosulfur Polymers

Copolymerization between elemental sulfur and unsaturated alkenes has been widely studied to prepare sulfur-enriched copolymers. When alkenes are copolymerized with ring-opened sulfur forming C—S bonds, the resulting copolymers can be used as active cathodes for Li–S batteries. Cross-bonding and strong chemical interactions of sulfur with carbon can effectively suppress the dissolution of polysulfides. For instance, Chung *et al.*[10] described an effective method to prepare sulfur-rich chemically stable polymeric materials by copolymerizing sulfur with 1,3-diisopropenylbenzene (DIB) (Figure 6a). The general strategy involved adding sulfur to a glass vial under magnetic stirring in an oil bath which was heated to 185 °C in order to open the sulfur rings (Figure 6b). Then the copolymer (S-DIB) was cooled to room temperature after adding DIB directly under stirring for 8–10 min. The resulting red-color S-DIB, was used as an electrochemically active sulfur reservoir material, which exhibited a high discharge capacity of 1100 mAh g^{-1} and long-term cycling performance of 823 mAh g^{-1} after 100 cycles at 0.1 C. Hu *et al.*[54] further improved the performance by infiltrating S–DIB into the AAO@CNT (Figure 6c), which was then sequentially washed by CS_2 and etched by NaOH (Figure 6d), affording a novel S-DIB@CNT hybrid cathode. The combination of physical and chemical confinement helped resolve the conductivity problem of S-r-DIB's, leading to enhanced cycling and rate performance with 880 mAh g^{-1} at 1 C after 100 cycles and a capacity retention of over 98%.

In another study, our group[55] directly vulcanized a thiourea aldehyde resin (TAR) and formed TAR backbone structures that were highly crosslinked with sulfur (Figure 7a). The resulting sulfur-rich copolymer cp(S–TAR) comprised abundant mesopores, which provided short ion channels (good for Li^+ diffusion), leading to a high initial capacity of 1285 mAh g^{-1}. Moreover, the formation of C—S covalent bonds enhanced the cycling stability with an ultralow fading rate of 0.045% per cycle

Encyclopedia of Inorganic and Bioinorganic Chemistry, Online © 2011–2019 John Wiley & Sons, Ltd.

This article was published in the *Encyclopedia of Inorganic and Bioinorganic Chemistry* in 2019 by John Wiley & Sons, Ltd.
DOI: 10.1002/9781119951438.eibc2687

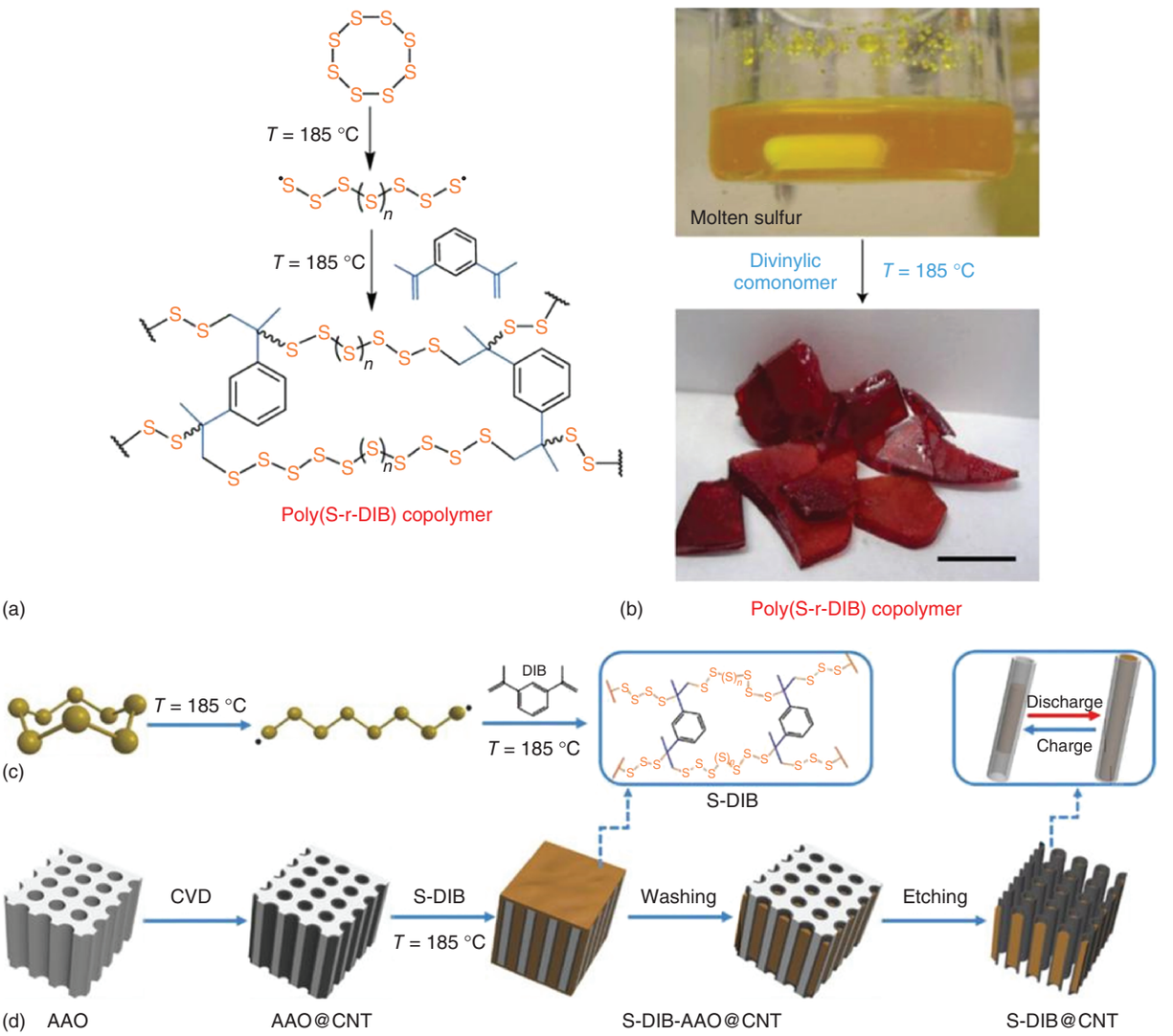

Figure 6 (a) Synthetic scheme for the copolymerization of S_8 with DIB to form chemically stable sulfur copolymers. (b) Images of liquid sulfur and poly(S-r-DIB) glass. (c) Synthesis scheme of S–DIB copolymer. (d) Schematic of the fabrication process of the S-DIB@CNT hybrid. [Panels (a,b) were reproduced with permission from Ref. 10. © 2013, Nature Publishing Group; panels (c,d) were reproduced with permission from Ref. 54, © 2017, Wiley-VCH Verlag GmbH & Co. KGaA]

and a Coulombic efficiency of 99% during the 500 deep discharge–charge cycles (Figure 7b).

The polymer matrices used above are electrically insulating, not ideal for maximizing the utilization of active sulfur and hence the rate performance. To alleviate these problems, Zentel and coworkers[56] directly copolymerized sulfur with allyl-terminated P3HT (poly(3-hexylthiophene-2,5-diyl)) (Figure 8a and b). The covalent bonds endowed S-P3HT with an enhanced battery performance, as compared to a simple mixture of sulfur and P3HT which were not covalently linked. Notably, uniform incorporation of P3HT with elemental sulfur can constitute an interpenetrating framework that is good for electron and ion transport in Li–S battery, which can also partially account for the enhanced battery performance. In another study, Fu *et al.* templated the vulcanization reaction by using an AAO array to synthesize vulcanized polyisoprene (PIP) nanowires (Figure 8c), which indeed facilitated Li^+ transport.[57] In addition, it was found that the electrochemical lithiation behavior of covalently bonded sulfur chains in polyisoprene (SPIP) were apparently different from that of isolated elemental sulfur molecules or macromolecules. Depending on the length of sulfur chain, different lithium sulfides, such as Li_2S, Li_2S_2, and other lower-order polysulfides (both reversible and irreversible) could be directly formed because lithiation

Encyclopedia of Inorganic and Bioinorganic Chemistry, Online © 2011–2019 John Wiley & Sons, Ltd.

This article was published in the *Encyclopedia of Inorganic and Bioinorganic Chemistry* in 2019 by John Wiley & Sons, Ltd.
DOI: 10.1002/9781119951438.eibc2687

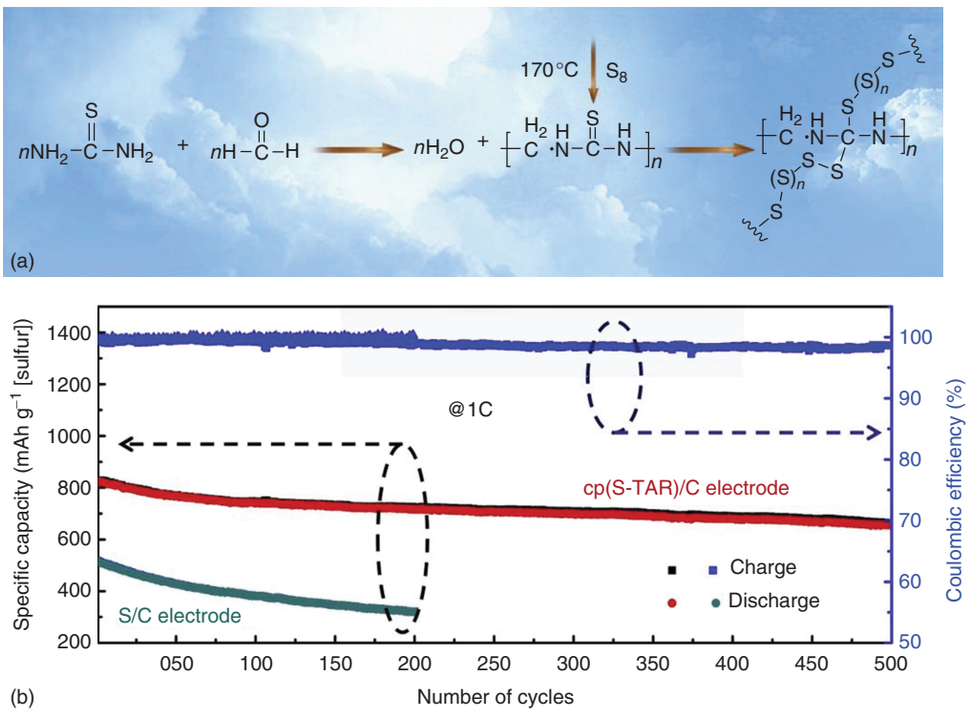

Figure 7 (a) Synthetic procedure of cp(S–TAR). (b) Long-term cycling performance and Coulombic efficiency for cp(S–TAR)/C and S/C cathodes at 1 C. [Reproduced with permission from Ref. 55, © 2018, Elsevier]

induced the cleavage of S—S bonds between the first and second S atoms in the sulfur chain. They also pointed out that the practical lithiation-delithiation reversibility might be contributed by the redistribution of the unanchored lithium sulfide species and the spatial confinement effects resulting from the crosslinked network, while the gradual capacity decay of SPIP cathodes was most likely due to the formation of irreversible C=S groups as well as thiol species during long-term charge–discharge cycling.

2.2.2 *Thiol-Derived Organosulfur Polymers*

Theoretically, thiol-containing molecules can also form covalent bonds with sulfur. For example, in practical applications, sulfur is widely used as an effective dehydrogenating reagent. Therefore, ring-opened sulfur can substitute the hydrogen in -SH to form S—S bonds, and the reaction mechanism for the synthesis of thiol-derived organosulfur polymers is somewhat similar to that for the alkene counterparts.[58] For instance, Park and coworkers[59] used trithiocyanuric acid (TTCA) crystals as soft templates to copolymerize with ring-opened sulfur through vulcanization. During heat treatment process, the crystallized TTCA was changed to porous frameworks, into which was impregnated with ring-opened sulfur followed by vulcanization (Figure 9a). Owing to the organized amine groups and covalent bonds in TTCA, the S-TTCA polymer showed an excellent discharge capacity of 945 mAh g^{-1} after 100 cycles at 0.2 C and a rate performance of 1210 mAh g^{-1} at 0.1 C, which was one of the highest specific capacities at that time. In order to enhance the performance of S-TTCA copolymer, Zou and coworkers[60] put TTCA into hollow carbon nanospheres (HCNs) with a high surface area of 2330 m^2 g^{-1} and large pore volume of 1.75 cm^3 g^{-1} and then vulcanized (Figure 9b). The HCNs–TTCA–S composite showed a high initial discharge capacity of 1430 mAh g^{-1} at 0.1 C, but a restricted rate and cycle performance. Hence, in order to enhance the distribution and electroconductibility, Chen's group[61] activated polymerization of sulfur and TTCA onto the surface of highly conductive rGO nanosheets (Figure 9c). Owing to the highly crosslinked organosulfur and excellent electrical conductivity of rGO, the composite showed a remarkable rate performance of 1341 mAh g^{-1} at 0.1 C and an enhanced battery cycling performance at a decay rate of only 0.0404% per cycle in 500 deep charge–discharge cycles, markedly better than those of similar copolymers. It is worth mentioning that the (S-TTCA)@rGO composite cathode had a higher loading of active sulfur at 2.0 mg cm^{-2} than those of other copolymers (~1.0 mg cm^{-2}), which is a suitable material for commercialization.

Encyclopedia of Inorganic and Bioinorganic Chemistry, Online © 2011–2019 John Wiley & Sons, Ltd.

This article was published in the *Encyclopedia of Inorganic and Bioinorganic Chemistry* in 2019 by John Wiley & Sons, Ltd.
DOI: 10.1002/9781119951438.eibc2687

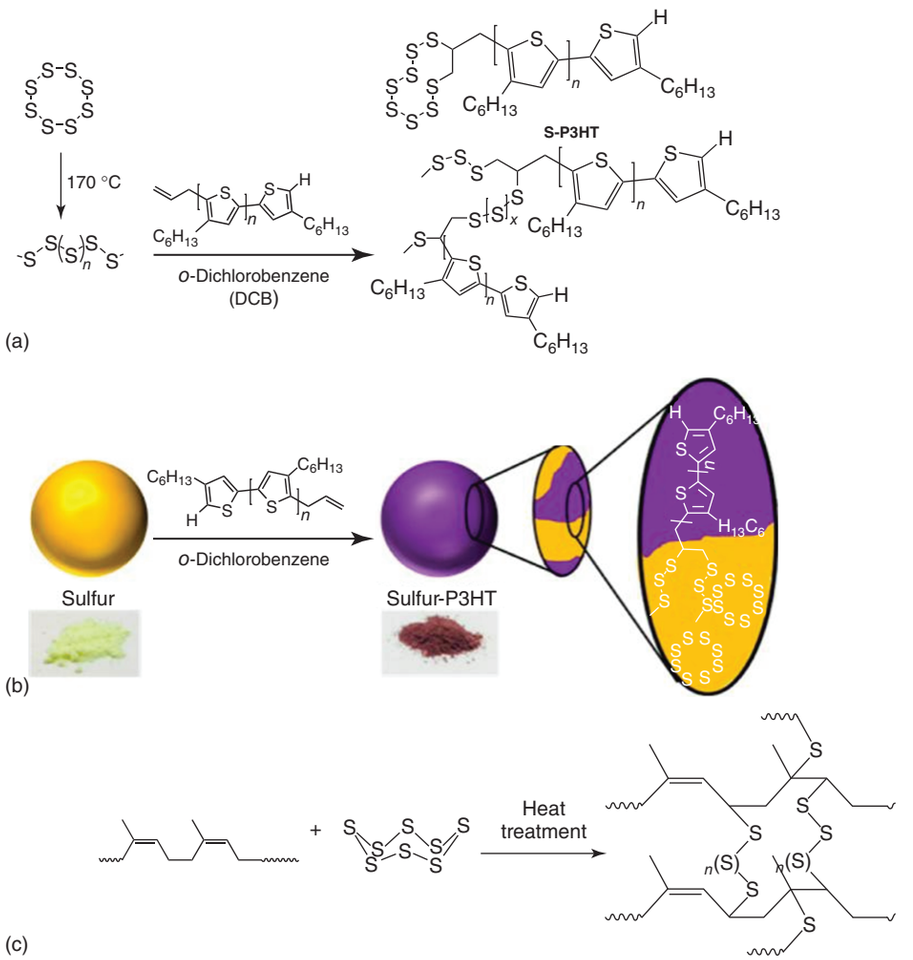

Figure 8 (a) Synthetic approach for the copolymerization of allyl-terminated P3HT and sulfur. (b) Proposed microstructure of the copolymer-containing sample. (c) Schematic of the vulcanization of PIP. [Panels (a,b) were reprinted with permission from Ref. 56. © 2015, American Chemical Society; panel (c) was reprinted with permission from Ref. 57. © 2016, American Chemical Society]

Inspired by Park's work,[59] Je *et al*. in 2016 reported an orthogonal, one-pot synthetic approach to secure elemental sulfur through thiol groups.[62] The sulfur chains are covalently linked to benzoxazine polymer (BOP) in a quantitative yield by reacting 4,4-dihydroxydiphenyldisulfide and hexahydro-1,3,5-triphenyl-1,3,5-triazine (Figure 10a). Owing to the homogeneous distribution of sulfur (in situ formation) and the C—S bonds, the S-BOP electrode delivered an appropriate cycling performance of 92.7% retention after 1000 cycles. Recently, Chen and coworkers[63] utilized m-aminothiophenol (MAT) to form conducting poly(m-aminothiophenol) (PMAT) with rich thiol groups. The resulting PMAT was then impregnated with molten elemental sulfur at 170 °C (Figure 10b) to form crosslinked sulfur side chains. Thanks to the highly crosslinked structure and high electrical conductivity of PMAT backbone, the cp(S–PMAT)/C cathode exhibited a high specific capacity (1240 mAh g^{-1} at 0.1 C, 880 mAh g^{-1} at 1 C and 600 mAh g^{-1} at 5 C) and robust cyclability (66.9% retention, where a capacity of 495 mAh g^{-1} was retained after 1000 cycles at a relatively high rate of 2 C).

2.2.3 *Nitrile-Derived Organosulfur Polymers*

Long-chain polysulfides can cause severe shuttling effects and affect the stability of Li–S batteries. One useful method to mitigate this issue is to decompose S_8 into small S_{2-4} molecules. Wang and coworkers prepared sulfur–polyacrylonitrile (SPAN) composites (sulfurized polyacrylonitrile) and observed good charge and ion transport behaviors that were needed for Li–S battery. Yet the chemical structure and electrochemical performance of SPAN remained under active debate. Wang and co-workers[64] argued that elemental sulfur was embedded

Encyclopedia of Inorganic and Bioinorganic Chemistry, Online © 2011–2019 John Wiley & Sons, Ltd.

This article was published in the *Encyclopedia of Inorganic and Bioinorganic Chemistry* in 2019 by John Wiley & Sons, Ltd.
DOI: 10.1002/9781119951438.eibc2687

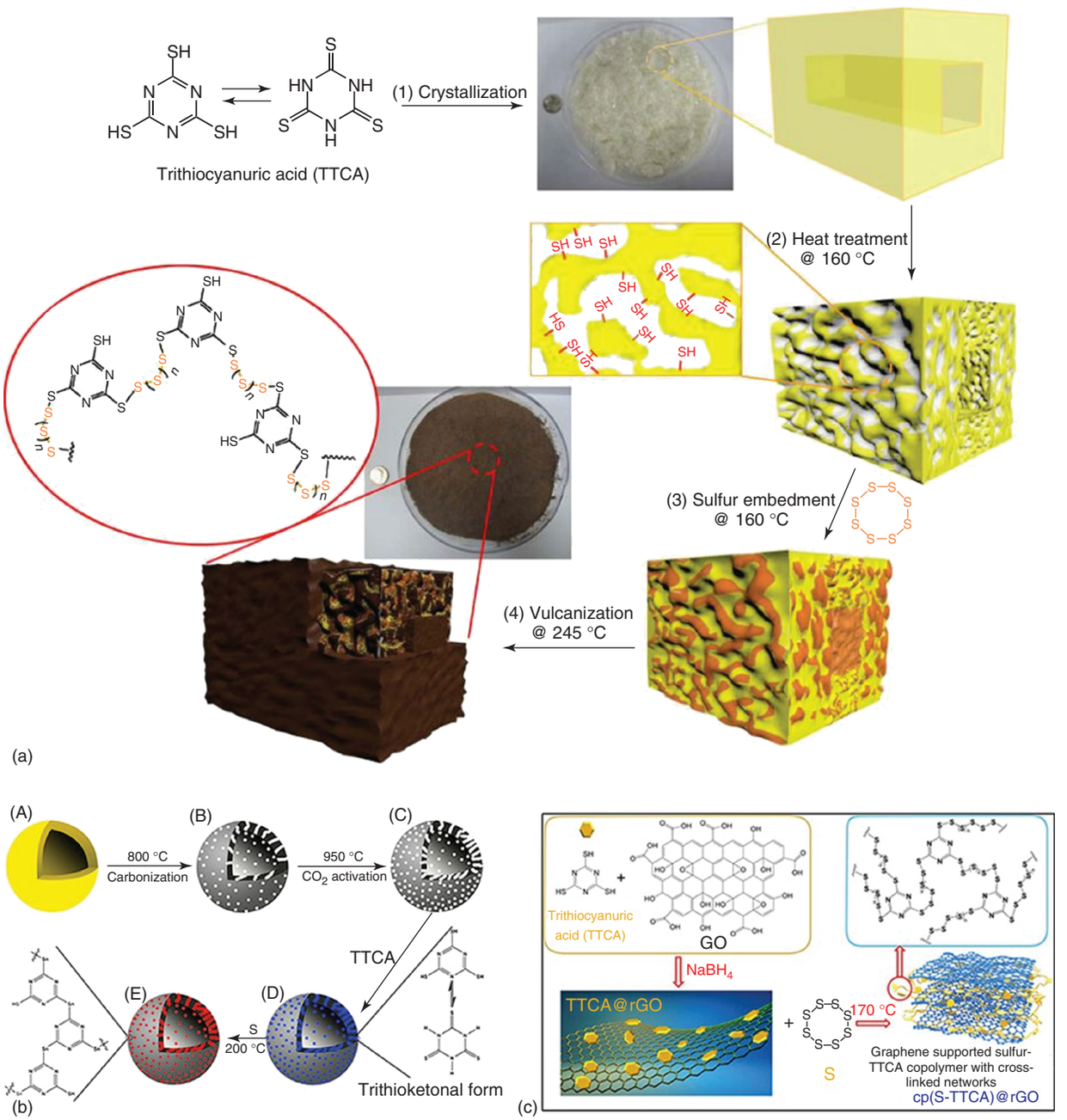

Figure 9 (a) Synthetic route of sulfur-rich polymers. Schematic drawings describing the synthetic procedures of sulfur-rich polymers with controllable morphology. (b) Schematic illustration of the preparation of HCNs and HCNs-TTCA-S. (c) Schematic illustration of the synthesis of graphene-supported highly crosslinked sulfur copolymer nanoparticles, cp(S-TTCA)@rGO. [Panel (a) was reproduced with permission from Ref. 59, © 2015, Nature Publishing Group; panel (b) was reproduced with permission from Ref. 60, © 2017, Elsevier; and panel (c) was reproduced with permission from Ref. 61, © 2017, Elsevier]

Encyclopedia of Inorganic and Bioinorganic Chemistry, Online © 2011–2019 John Wiley & Sons, Ltd.

This article was published in the *Encyclopedia of Inorganic and Bioinorganic Chemistry* in 2019 by John Wiley & Sons, Ltd.
DOI: 10.1002/9781119951438.eibc2687

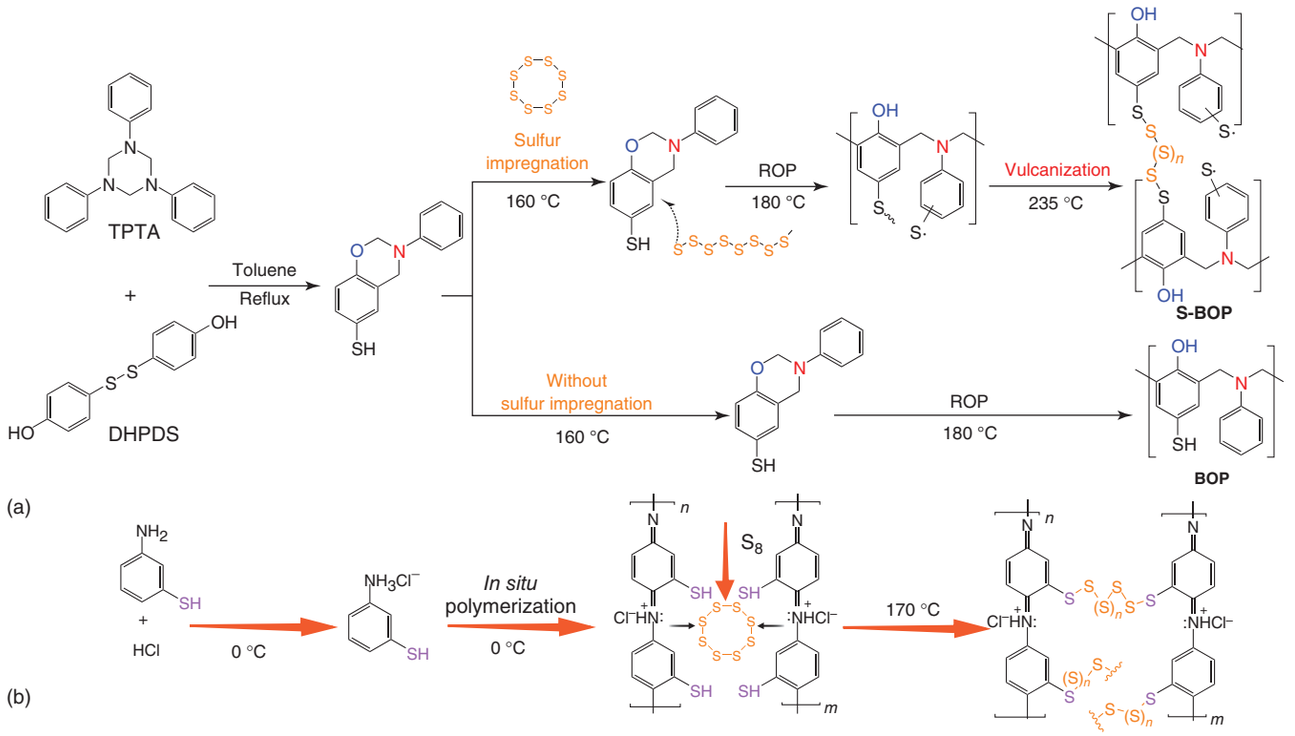

Figure 10 Synthetic procedures of (a) S-BOP copolymer and (b) cp(S-PMAT) copolymer. [Panel (a) was Reprinted with permission from Ref. 62. © 2016, American Chemical Society; panel (b) was reproduced with permission from Ref. 63. © 2017, Wiley-VCH Verlag GmbH & Co. KGaA]

in the pyrolyzed PAN (Figure 11a), whereas Yu *et al.*[65] and Fanous *et al.*[66] believed sulfur was covalently bonded onto the PAN backbones in the form of short -S_x- chains (Figure 11b and c). In 2014, Zhang *et al.*[67] demonstrated that the structures reported by Yu and Fanous were inaccurate because of inconsistency of the resulting of *C*/*H* ratio and the correct one was the one shown in Figure 11d.

Recently, Wang's group[52] synthesized PAN nanoparticles, less than 100 nm in size, on the surface of graphene nanosheets (GNS) by a simple in situ method, followed by sulfurization (Figure 12a). Because the as-synthesized pPAN–S particles had an intimate contact with GNS and could be well-dispersed on GNS, the electrochemical measurements of the pPAN–S/GNS composite cathode showed an excellent discharge capacity of ca.1500 mAh g^{-1} (corresponding to ca. 90% sulfur utilization) and a competitive capacity of ca. 800 mAh g^{-1}, even at up to 6 C. More recently, a highly ordered mesoporous sulfurized polyacrylonitrile (MSPAN) was obtained by directly heating a SBA-15 template embedded with sulfur followed by removal of SBA-15 templates with acidic etching (Figure 12b).[68] The resulting composite MSPAN provided a large surface area and abundant porous structures. The corresponding nanocomposite cathode exhibited a stable cycling property with 610 mA h g^{-1} after 900 cycles at 2 C (Figure 12c). Even at 5 C, the MSPAN-based cathode could also display reasonable capacity retention.

In 2015, Coskun and coworkers[69] prepared S-CTF-1 (covalent triazine framework) through a catalyst- and solvent-free method without using any external templates where elemental sulfur was incorporated onto 1,4-dicyanobenzene at 400 °C. The resulting copolymer S-CTF-1 constituted a macrocycle backbone with multiple sulfur side chains (Figure 13a). When used as cathode in Li–S batteries, it exhibited an apparent electrochemical performance, with 85.8% capacity retention after 300 cycles along with a high initial Coulombic efficiency (ICE) of ca. 94.4% at 0.05 C. In order to further improve the electrochemical performances, Xu *et al.*[70] introduced electronegative fluorine onto the CTF (Figure 13b). The polar fluorine species was argued to serve as anchoring sites for chemical adsorption of polysulfides, and hence suppress the dissolution and accelerate the conversion of polysulfides. As a result, the fluorinated porous triazine-based frameworks (FCTF)-S showed a superior performance as compared to CTF–S without fluorine, with an initial discharge capacity of 1296 mA h g^{-1} at 0.1 C and a retention of 833 mA h g^{-1} after 150 cycles at 0.5 C.

Encyclopedia of Inorganic and Bioinorganic Chemistry, Online © 2011–2019 John Wiley & Sons, Ltd.

This article was published in the *Encyclopedia of Inorganic and Bioinorganic Chemistry* in 2019 by John Wiley & Sons, Ltd.
DOI: 10.1002/9781119951438.eibc2687

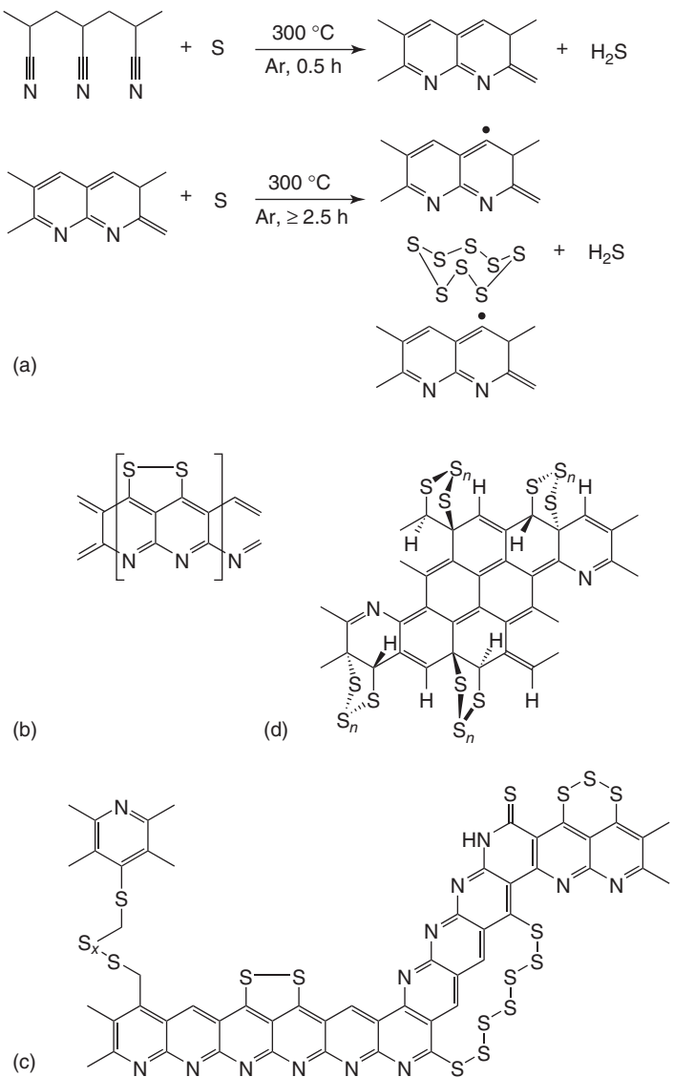

Figure 11 (a) Schematic of the thermo-reaction between PAN and sulfur. Possible molecular structures of SPAN according to Yu's (b) and (c) Fanous's reports. (d) Revised structure of SPAN proposed by Zhang, matching the results of *C*/*H* ratio in SPAN. [Panel (a) was reproduced with permission from Ref. 64, © 2003, Wiley-VCH Verlag GmbH & Co. KGaA; panel (b) was reproduced with permission from Ref. 65, © 2004, Elsevier; panel (c) was reprinted with permission from Ref. 66, © 2011, American Chemical Society; panel (d) was reproduced with permission from Ref. 67, © 2014, MDPI]

2.3 Incorporation of Polar Compounds

In addition to the above physical confinement and covalent bonding strategies, recent studies have also shown that chemical binding of polysulfides is an important, novel strategy to improve the performance of Li–S batteries. In theory, an ideal chemical binding material should be able to selectively control the shuttling of polysulfide anions via strong bonding interactions between them, while not disturbing Li^+ ion transfer. Developing a lightweight and chemically selective host materials is therefore of urgent importance. In the following section, we will summarize the commonly used polar anchoring materials for tailoring the performance of Li–S batteries.

2.3.1 Heteroatom-Doped Nanocarbon

It was first recognized by Zhang *et al.*[71] that the weak Van der Waals' (vdW) interaction between the intrinsic nonpolar carbon-based matrix materials and polar Li_2S_x species could only provide weak confinement, hence detachment of Li_2S_x species from the carbon matrix surface usually occurred, and their further diffusion into electrolyte caused rapid degradation in capacity

Encyclopedia of Inorganic and Bioinorganic Chemistry, Online © 2011–2019 John Wiley & Sons, Ltd.

This article was published in the *Encyclopedia of Inorganic and Bioinorganic Chemistry* in 2019 by John Wiley & Sons, Ltd.
DOI: 10.1002/9781119951438.eibc2687

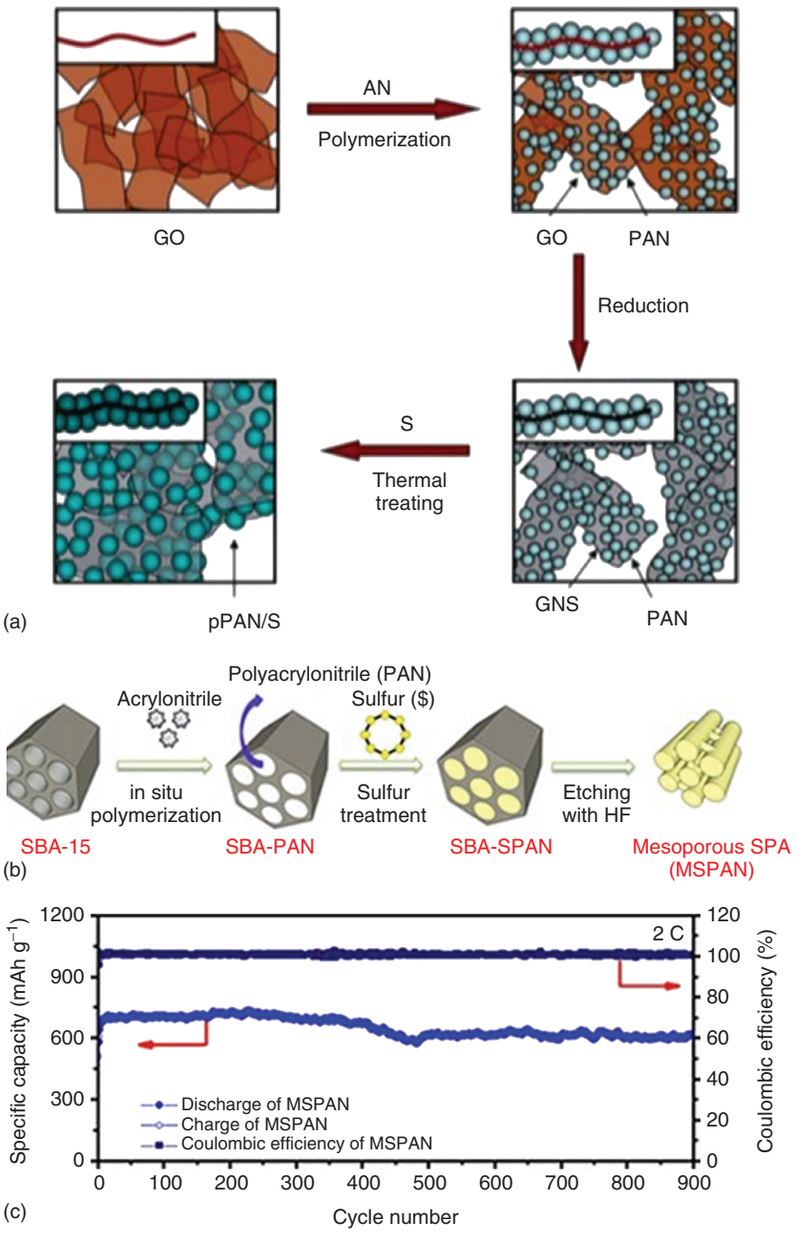

Figure 12 (a) Illustration of in situ polymerization and synthesis of pPAN-S/GNS. (b) Schematic diagram of the sequential fabrication steps for MSPAN. (c) Cycling performance and Coulombic efficiency of MSPAN cell at 2 C rate. [Panel (a) was reproduced with permission from Ref. 52, © 2014, Wiley-VCH Verlag GmbH & Co. KGaA; panels (b,c) were reprinted with permission from Ref. 68. © 2017, American Chemical Society]

and rate performance. Intuitively, heteroatom doping should change the electronic state of carbon surface and hence modify the polarity of carbon matrix. A systematic density functional theory (DFT) calculation suggested that chemical modification with N or O dopant significantly enhanced the interaction between the carbon matrix and Li_2S_x species via electrostatic attraction and thereby effectively prevented the appearance of polysulfides shuttle, enabling a high discharge capacity and a high Coulombic efficiency.[72] Moreover, both N and O heteroatoms with extra pairs of electrons were considered as electron-rich donors that naturally served as a Lewis base sites to effectively interact with strong Lewis acid of Li terminal atoms in Li_2S_x species via dipole–dipole electrostatic interaction. In contrast, the monodoping of B, F, S, P, or Cl into the carbon matrix

Encyclopedia of Inorganic and Bioinorganic Chemistry, Online © 2011–2019 John Wiley & Sons, Ltd.

This article was published in the *Encyclopedia of Inorganic and Bioinorganic Chemistry* in 2019 by John Wiley & Sons, Ltd.
DOI: 10.1002/9781119951438.eibc2687

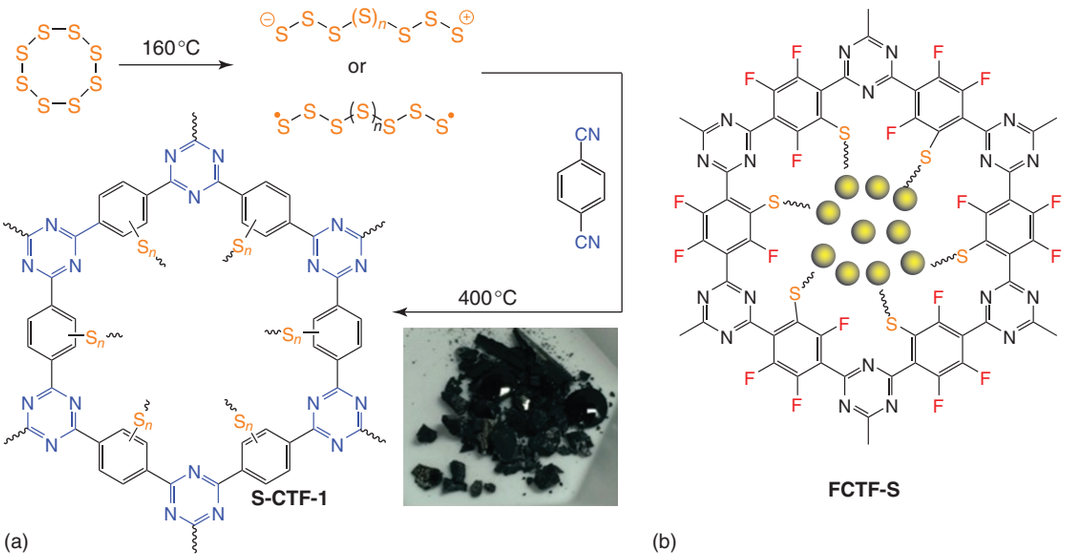

Figure 13 (a) Synthesis procedure of S-CTF-1 and an optical image of S-CTF-1. (b) Chemical structure of FCTF-S. [Panel (a) was reproduced with permission from Ref. 69, © 2016, Wiley-VCH Verlag GmbH & Co. KGaA; panel (b) was reprinted with permission from Ref. 70. © 2017, American Chemical Society]

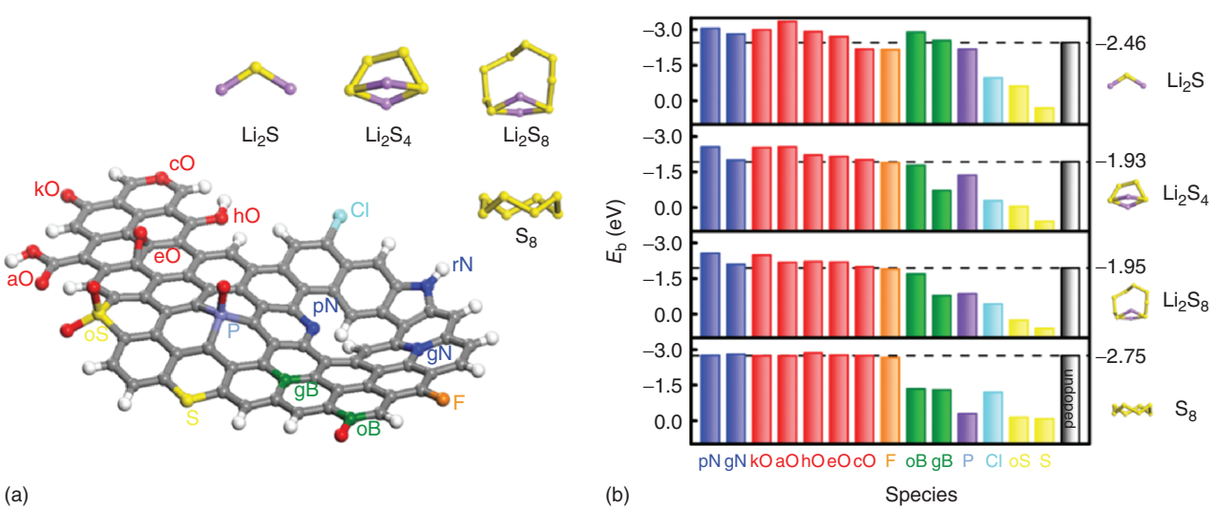

Figure 14 (a) Schematic diagram of *X*-doped nanocarbon materials (X = N, O, F, B, P, S, Cl) and PBE level optimized structure of Li_2S, Li_2S_4, Li_2S_8, and S_8 molecules, which are key intermediates in the charge/discharge process of Li–S battery. (b) Binding energy E_b (eV) of Li_2S, Li_2S_4, Li_2S_8, and S_8 interacting with *X*-doped GNRs with zigzag edge, and binding energies of Li_2S, Li_2S_4, Li_2S_8, and S_8 interacting with pristine (undoped) GNR are shown as grey bars and dashed lines for reference. Carbon, hydrogen, nitrogen, oxygen, fluorine, boron, phosphorus, chlorine, lithium, and sulfur elements are represented by grey, white, blue, red, orange, green, lavender, cyan, purple, and yellow, respectively. [Reprinted with permission from Ref. 72, © 2016, Wiley-VCH Verlag GmbH & Co. KGaA]

was unsatisfactory, in terms of the strength of electrostatic interaction with Li terminal atoms in Li_2S_x species.

Subsequently, theoretical calculations were conducted to determine the binding energy (E_b) of the series of doping elements in different doping configurations. From the results showed in Figure 14, the principles for the rational design of doped carbon scaffolds to achieve strong coupling with Li_2S_x species in Li–S batteries can be summarized as follows: (i) doping atom has a lone pair electron; (ii) doping atom exhibits a higher electronegativity than carbon and a small radius that matches Li; (iii)

Encyclopedia of Inorganic and Bioinorganic Chemistry, Online © 2011–2019 John Wiley & Sons, Ltd.

This article was published in the *Encyclopedia of Inorganic and Bioinorganic Chemistry* in 2019 by John Wiley & Sons, Ltd.
DOI: 10.1002/9781119951438.eibc2687

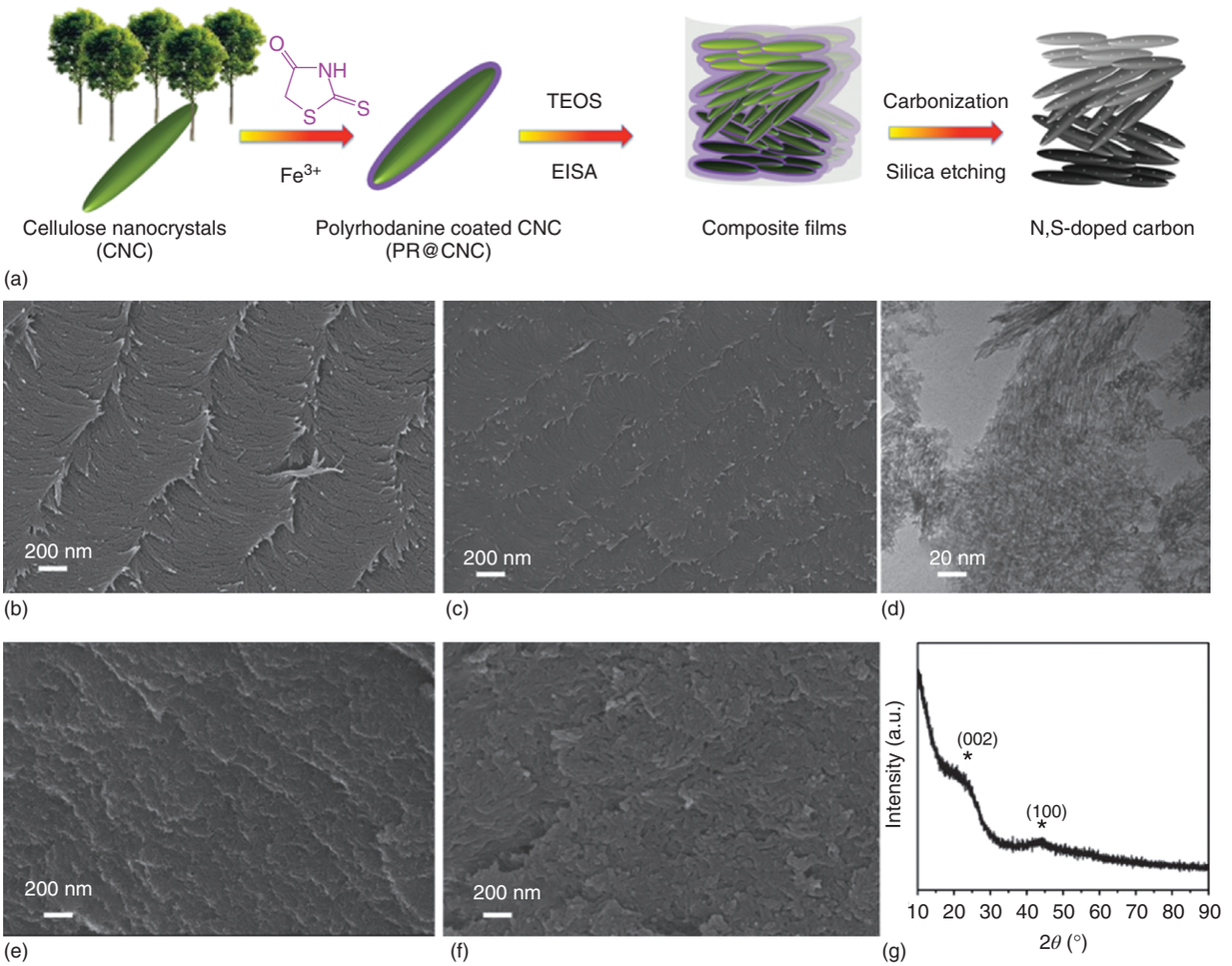

Figure 15 (a) Schematic illustration of the synthesis of nitrogen/sulfur-doped cellulose (NSC); (b) SEM images of periodic self-assembled cellulose nanocrystals (CNCs) and (c) PR@CNC precursors for the synthesis of CDC and NSC, respectively; (d) TEM and (e) SEM images of NSC; (f) SEM image of the NSC/S-70 composite; (g) XRD pattern of the NSC. [Reprinted with permission from Ref. 73, © 2015, Wiley-VCH Verlag GmbH & Co. KGaA]

doping atom forms a delocalized π bond with the conjugated system; and (iv) doping atom forms a stable bond to the carbon plane. With the fulfillment of these conditions, the carbon matrix could form a strong electrostatic dipole–dipole interaction with Li_2S_x species, coinciding with the theoretical and experimental results that N or O doping is a better choice to relieve the shuttle effect.

In another work, Pang *et al.*[73] developed a strategy based on strong chemisorption of polysulfides utilizing an ordered nanoporous carbon dual-doped with nitrogen and sulfur (Figure 15). The doped carbon was synthesized from self-templating of biomaterial-derived cellulose nanocrystals and exhibited a tunable hierarchically porous structure as well as high surface area. The dual doping with N and S atoms of the porous carbon remarkably enhanced the chemisorption of lithium polysulfides. XPS studies revealed a synergistic N–Li and S–S interactions. The binding configuration was also confirmed by ab initio DFT calculations, where Li^+ and doped N atoms formed Li–N chemical bond while the polysulfide anions and doped S atoms formed S–S. In addition, the electrical conductivity of the porous carbon was greatly improved, as compared to undoped carbon. Using this dual-doped carbon as a sulfur host, the sulfur electrode was able to deliver a high capacity of 1370 mAh g^{-1} at 0.05 C and discharge/charge for 1100 cycles at 2 C rate with a very low capacity fading rate of 0.052% per cycle. These results demonstrated that a synergistic functionalization of intrinsic carbons with nitrogen and sulfur heteroatoms dramatically modified the electron density distribution of the host carbons substrate, leading

Encyclopedia of Inorganic and Bioinorganic Chemistry, Online © 2011–2019 John Wiley & Sons, Ltd.

This article was published in the *Encyclopedia of Inorganic and Bioinorganic Chemistry* in 2019 by John Wiley & Sons, Ltd.
DOI: 10.1002/9781119951438.eibc2687

to much stronger polysulfide binding than that for undoped or nitrogen mono-doped carbons.

Besides heteroatom doping, direct incorporation of nitrogen-rich polar materials is also proven to be effective for polysulfides anchoring/binding. Pang and Nazar[74] reported that introduction of a light-weight nanoporous graphitic carbon nitride (high-surface-area g-C_3N_4) into sulfur cathode enabled an ultralow capacity fading rate of only 0.04% per cycle over 1500 long-term cycles at a practical rate of 0.5 C. On the basis of the results from spectroscopic studies and first-principles theoretical calculations, they pointed out that the ultrahigh concentration of accessible pyridinic nitrogen (up to 53.5 at%) of g-C_3N_4 acted as strong chemisorption sites for lithium polysulfides, which accounted for the greatly improved cycling performance, as compared to that of N-doped or undoped carbons.

2.3.2 *Transition Metal Sulfides*

With the advancement in the synthesis methods of 2D dichalcogenides in recent years, various transition metal sulfides have been explored for Li–S batteries.[75] As compared with carbon-based materials, transition metal sulfides demonstrate several advantages, such as (i) low lithiation voltages vs Li/Li^+, which is outside of the working voltage window of Li–S batteries; (ii) a strong sulfiphilic property toward the Li_2S_x species; and (iii) there are a large number of metallic or half-metallic phases of metal chalcogenides, such as pyrite, spinel, and NiAs structures, which are highly electronically conductive. Many transition metal sulfides have been proposed as polysulfide-anchoring materials, considering their polarity and electrical conductivity. For example, TiS_2 was the earliest light-weight intercalating cathode material to be used in secondary lithium batteries,[76] and exhibited a high diffusion rate of lithium ions and high electronic conductivity. With its polar surface a relatively stable sulfur cathode comprised of TiS_2 host was prepared by Archer and coworkers,[77] showing a marked capacity of about 17 mAh cm^{-2} after 100 cycles with a high sulfur loading of 40 mg cm^{-2}. They also performed DFT calculations and found that the binding energy between lithium polysulfides and TiS_2 was about 2.60 eV, which is nearly three times greater than that between lithium polysulfides and polyacrylonitrile and around 10 times higher than that between lithium polysulfides and carbon-based graphene.[78] This strong chemical interaction between lithium polysulfides and TiS_2 host significantly alleviated the dissolution of polysulfides into electrolytes and hence enabled an improved cycling performance.

Actually, TiS_2 was theoretically proven to be an ideal chemical anchoring material for polysulfides by Cui's group.[71] They used a first-principles method with vdW interaction included to systematically investigate the adsorption of different Li_2S_x species on transition metals-based 2D layered materials (e.g., oxides, sulfides, and chlorides), and study the detailed interaction and electronic structure, including binding strength, configuration distortion, and charge transfer. The resulting simulated binding energies (E_b) with vdW correction at different lithiation stages are shown in Figure 16, where one can find that for the adsorption of pristine S_8, all the investigated materials show a small binding energy in the range of 0.75–0.85 eV, which is very comparable to that for graphene, regardless of crystalline graphene (c-G) and amorphous graphene (a-G) (Figure 16a). However, when lithiation starts, the binding energy for the

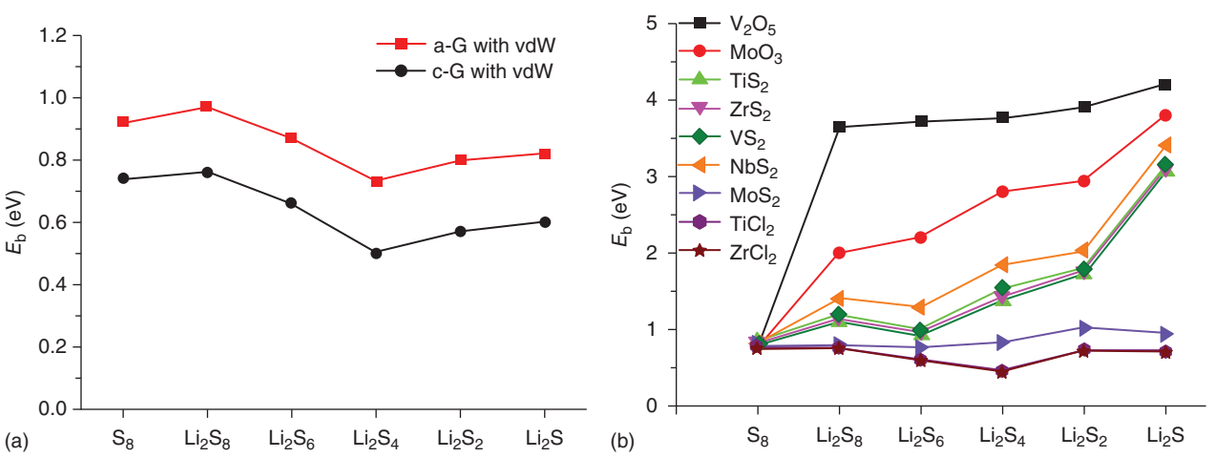

Figure 16 Variation of binding energies of lithium sulfides at four different lithiation stages (S_8, Li_2S_6, Li_2S_4, and Li_2S_2) on various anchoring materials. (a) a-G and c-G; and (b) different layered transitions metal compounds. [Reprinted with permission from Ref. 71. © 2015, American Chemical Society]

Encyclopedia of Inorganic and Bioinorganic Chemistry, Online © 2011–2019 John Wiley & Sons, Ltd.

This article was published in the *Encyclopedia of Inorganic and Bioinorganic Chemistry* in 2019 by John Wiley & Sons, Ltd.
DOI: 10.1002/9781119951438.eibc2687

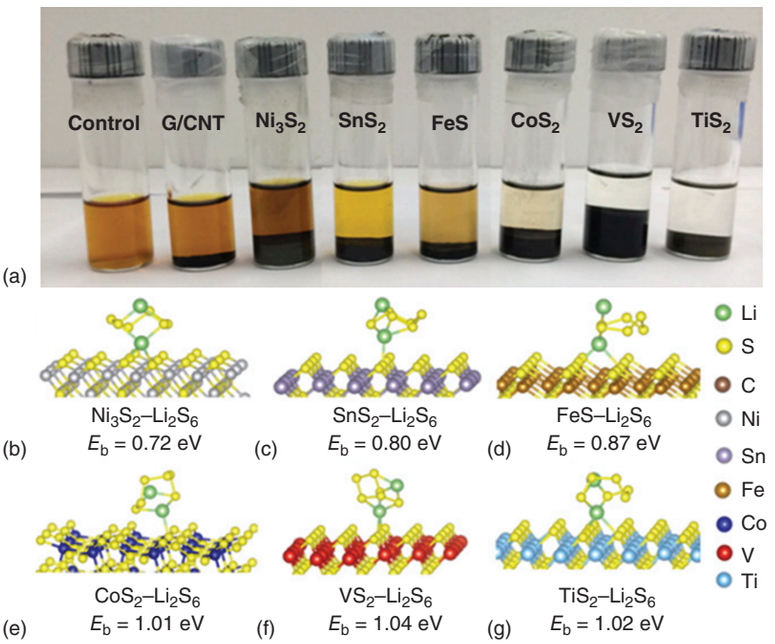

Figure 17 Lithium polysulfide (Li_2S_6) adsorption by carbon and metal sulfides and corresponding simulation of Li_2S_6 adsorbed on the surface of metal sulfides. (a) Digital image of the Li_2S_6 (0.005 M) captured by carbon and metal sulfides in a DOL/DME solution. Atomic conformations and binding energy for Li_2S_6 species adsorption on (b) Ni_3S_2, (c) SnS_2, (d) FeS, (e) CoS_2, (f) VS_2, and (g) TiS_2. Here, green, yellow, gray, purple, brown, blue, red, and cyan balls represent lithium, sulfur, nickel, tin, iron, cobalt, vanadium, and titanium atoms, respectively. [Reprinted with permission from Ref. 80, © 2017, National Academy of Sciences]

different materials varies (Figure 16b). For V_2O_5 and MoO_3, the binding energies of both oxides are higher than 2.0 eV over the whole lithiation process. For the chlorides ($TiCl_2$ and $ZrCl_2$), their E_b is lower than 0.80 eV. For most of the sulfides, including MoS_2, TiS_2, ZrS_2, NbS_2, and VS_2, their binding energies are moderate, not so high as that for oxides, but much higher than that for chlorides. Specifically, except for MoS_2, all the sulfides shown in Figure 16 demonstrate an E_b value higher than 1.00 eV. Figure 16 also reveals that the evolution trend of E_b with lithiation process for transition metal chlorides is similar to that of graphene, but opposite to that for both transition metal oxides and sulfides during lithiation. Because the E_b continuously increases for both transition metal oxides and sulfides as lithiation proceeds, the anchoring effect of these two kinds of materials should mainly derive from their chemical interaction with the Li atoms by forming Li—S and Li—O bonds on transition metal sulfides and oxides, respectively. In contrast, the weak anchoring effect between chlorides and Li_2S_x species is mainly attributed to the vdW interaction.

From the viewpoint of anchoring effect, a higher E_b enables a stronger binding strength for Li_2S_x species. However, anchoring materials with too strong binding strength (such as V_2O_5 and MoO_3) cause the break of Li—S bonds in Li_2S_x species, leading to the formation of isolated Li^+ and S^{2-} ions, which can be readily dissolved into the electrolyte. Moreover, the decomposition of Li—S bonds in Li_2S_x species will impair the effect of sulfur, which is the key functional material that imparts the high capacity to the cathode of Li–S batteries. Therefore, too strong anchoring materials such as V_2O_5 and MoO_3, with a binding energy higher than 2.0 eV, might not be good candidates, while those with a moderate binding energy can maintain a balance between binding strength and integrity of the Li_2S_x species, overcoming the inherited disadvantages of both too strong and too weak anchoring materials. These findings can explain very well why anchoring materials with a medium binding energy, including TiS_2, ZrS_2, and VS_2, can show superior cycling performances to many oxide materials.[79]

In a subsequent experimental study,[80] Zhou *et al.* confirmed that transition metal sulfides based moderate-strength anchoring materials such as TiS_2, VS_2, and CoS_2, could effectively anchor Li_2S_6. As shown in Figure 17(a), after prolonged contact with Li_2S6, nonpolar G/CNT had no apparent effect on adsorbing polysulfides as the color of the solution remained the same as that of the control sample, indicating only weak physical adsorption for G/CNT sample. In contrast, FeS and SnS_2 both demonstrated higher adsorption capability of Li_2S_6, as compared to

Encyclopedia of Inorganic and Bioinorganic Chemistry, Online © 2011–2019 John Wiley & Sons, Ltd.

This article was published in the *Encyclopedia of Inorganic and Bioinorganic Chemistry* in 2019 by John Wiley & Sons, Ltd.
DOI: 10.1002/9781119951438.eibc2687

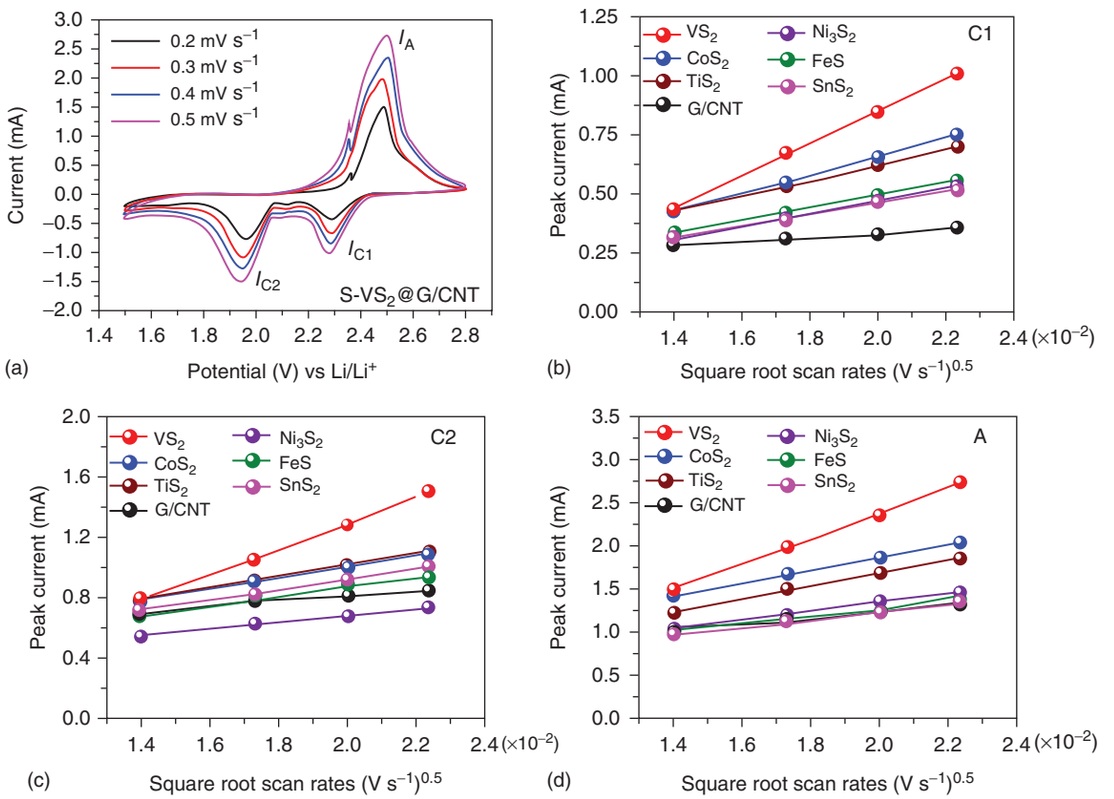

Figure 18 (a) CV curves of the sulfur cathode employing various anchoring materials at different scan rates. CV peak current for the (b) first cathodic reduction process (I_{C1} : $S_8 \rightarrow Li_2S_x$); (c) second cathodic reduction process (I_{C2} : $Li_2S_x \rightarrow Li_2S_2/Li_2S$); and (d) anodic oxidation process (I_A : $Li_2S_2/Li_2S \rightarrow S_8$) against the square root of scan rates. [Adapted with permission from Ref. 80, © 2017, National Academy of Sciences]

G/CNT,[81] whereas Ni_3S_2 exhibited lower adsorption, as demonstrated by the lack of any significant color change (Figure 17b–d). Notably, the originally yellow-colored polysulfide solution became colorless after the addition of TiS_2 or VS_2, and became much lighter in color for CoS_2, suggesting a strong interaction between Li_2S_6 and these sulfide hosts (the binding energy was about 1.0 eV for Li_2S_6) (Figure 17e–g).

In addition to the above anchoring effect, Zhou *et al.*[80] discovered that some of the transition metal sulfides were able to serve as an activation catalyst to facilitate the oxidation of the discharge product, Li_2S, back to the charge product, S_8. Specifically, from the cyclic voltammetry (CV) curves of a sulfur cathode employing SV_2 as the anchoring materials (Figure 18a), one can see two cathodic peaks at around 2.30 V (denoted as I_{C1}) and 1.95 V (denoted as I_{C2}), due to the reduction of S_8 to long-chain lithium polysulfides ($S_8 \rightarrow Li_2S_x$) and the subsequent formation of short-chain Li_2S_2/Li_2S ($Li_2S_x \rightarrow Li_2S_2/Li_2S$), respectively. Accordingly, the anodic peak at around 2.50 V (denoted as I_A) derives from the conversion of short-chain Li_2S_2/Li_2S to long-chain polysulfides and finally S_8 ($Li_2S_2/Li_2S \rightarrow S_8$). The heights of these three current peaks (I_{C1}, I_{C2}, I_A) show a linear correlation with the square root of potential scanning rate of all the investigated electrodes employing various anchoring materials (Figure 18b–d), signifying a diffusion-limited process. Therefore, the lithium diffusion process can be approximately described with the classical Randles–Sevcik equation,[82,83] $I_p = (2.69 \times 10^5) n^{3/2} S (D_{Li^+})^{1/2} C_{Li^+} v^{1/2}$, where I_p is the corresponding peak current of the CV curve, n corresponds to the charge transfer number, S is the geometric surface area of the active part of the working electrode, D_{Li^+} is the diffusion coefficient of Li^+, C_{Li^+} is the concentration of Li^+ in sulfur cathode, and v is the electrode potential scanning rate. From the linear plots depicted in Figure 18(b)–(d), one can find that the carbon-based G/CNT anchoring material displays the smallest slopes and hence shows the lowest lithium ion diffusivity, which is attributed to the weak adsorption of Li_2S_x species and inefficiency in catalyzing Li_2S conversion, probably caused by the high viscosity of Li_2S_x in electrolyte, or the deposition of a thick nonconductive layer on electrode surface. By contrast, the electrodes with VS_2, CoS_2, or TiS_2 exhibit much faster Li^+

Encyclopedia of Inorganic and Bioinorganic Chemistry, Online © 2011–2019 John Wiley & Sons, Ltd.

This article was published in the *Encyclopedia of Inorganic and Bioinorganic Chemistry* in 2019 by John Wiley & Sons, Ltd.
DOI: 10.1002/9781119951438.eibc2687

diffusion than G/CNT and also better redox kinetics than those electrodes with Ni_3S_2, SnS_2, and FeS, indicating that the introduction of moderate-strength polar metal sulfide hosts can efficiently catalyze the redox conversion of sulfur. The high Li^+ diffusivity on CoS_2, VS_2, and TiS_2 is also supported by their simulation results, where graphene showed the highest Li^+ diffusion barrier of about 0.30 eV, while for Ni_3S_2, SnS_2, and FeS, the Li^+ diffusion barriers were lower but about 0.1 eV larger than those for CoS_2, VS_2, and TiS_2. Therefore, the requirements for a suitable anchoring material in the cathode should include: (i) a moderate binding energy with Li_2S_x species; (ii) capability in rational control of Li_2S deposition; (iii) fast Li^+ diffusion ability; and (iv) efficient catalytic conversion of the sulfur redox. These requirements can help decrease electrode polarization, increase active sulfur utilization, and improve rate performance and the charge–discharge cycling stability.

Moreover, pyrite CoS_2 was also proven to have high catalytic activity in polysulfide reduction by Jin and coworkers.[84] The pyrite type CoS_2 crystal has marked electronic conductivity of 6.7×10^3 S cm^{-1} at 300 K. Yuan *et al.* incorporated the sulfiphilic half-metallic pyrite-type CoS_2 into the cathode of Li–S battery to facilitate the conversion process of polysulfide redox[85] by mixing CoS_2 with graphene and sulfur at different ratios. CV measurements showed that the current density significantly increased by an order of magnitude as the content of CoS_2 was increased from 0 to 30 wt%, demonstrating that the interactions of CoS_2–polysulfides not only statically existed but also dynamically accelerated the electrochemical reactions of Li_2S_x. Electrochemical impedance spectroscopic (EIS) tests revealed that charge transfer at the CoS_2–polysulfide interface was much faster than that at the graphene–polysulfide interface, and the redox kinetics of polysulfides in liquid phase ($Li_2S_8 \leftrightarrow Li_2S_6 \leftrightarrow Li_2S_4$) were also improved after introduction of sulfiphilic CoS_2 hosts. Along this line, hierarchically porous CoS_2/carbon composite paper was developed and applied as an interlayer for capturing lithium polysulfides through physical absorption and also chemical binding in a working Li–S battery.[86] The corresponding composite CoS_2/C/S cathode was able to deliver a high initial sulfur utilization of 74% at 0.2 C and demonstrate a long cycling life.

In addition to the transition metal sulfides discussed above, recently 3D interconnected graphene-like Co_9S_8 nanosheets were synthesized through a microwave-assisted solvothermal method by Pang *et al.*[87] Co_9S_8 is a member of the Pentlandite family, with a particularly high room-temperature electrical conductivity of 290 S cm^{-1}. In contrast to results in earlier studies where only Li–S (or Li–O) binding between the Li atoms in Li_2S_x species and the layered metal sulfide (oxide) was observed, a strong synergistic binding effect from both Li and S ions in Li_2S_x species was confirmed. The chemical binding of positively charged Li^+ to S^{2-} of Co_9S_8 and the terminal sulfur to Co (if available) completely dominated the interaction between Co_9S_8 and Li_2S_4, where the binding energy of 6.93 eV (vdW interactions included) was the highest ever reported for Li_2S_x on an anchoring material surface to date.

2.3.3 *Transition Metal Nitrides*

Sun *et al.*[88] prepared a conductive porous vanadium nitride nanoribbon/graphene composite (VN/G) as the cathode material of a Li–S battery, where the shuttle effect of lithium polysulfides was drastically diminished. The fabrication process of a VN/G composite and cell assembly were schematically shown in Figure 19. The 3D free-standing structure composed of a graphene network facilitated the electrolyte absorption and the transport of electrons and ions. In addition, VN showed a strong anchoring effect for polysulfides and its high conductivity also accelerated the polysulfide conversion. The VN/G-based sulfur cathode delivered an excellent initial discharge capacity of 1471 mAh g^{-1}, and more importantly, it was able to maintain a stable cycling performance with a Coulombic efficiency above 99.5% for 100 charge–discharge cycles at 0.2 C, indicating that dissolution of polysulfides into the organic electrolyte was largely mitigated in the VN/G electrode.

In addition, Cui *et al.*[89] reported the use of a mesoporous TiN–S cathode to improve the performance of Li–S batteries. The TiN–S composite was synthesized by a melt-diffusion method that encapsulated the sublimed sulfur in mesoporous TiN that was produced by a solid–solid phase separation method with zinc titanate as a starting material. Benefiting from the high electrical conductivity, robust porous frameworks and favorable adsorption properties of TiN, the TiN–S composite cathode exhibited a high specific capacity and excellent rate capability. More importantly, compared with mesoporous TiO_2–S and Vulcan C–S composite cathodes, the TiN–S composite cathode displayed the best cycling stability, with a capacity degradation rate of only 0.07% per cycle over 500 charge/discharge cycles. The excellent electrical conductivity and the chemical binding of the soluble intermediate species of mesoporous TiN allow for high rate of charge/discharge.

In another study, Mosavati *et al.*[90] prepared three different transition metal nitrides (WN, VN, and Mo_2N) as cathode materials for Li–S batteries (Figure 20). Among these materials, WN demonstrated the most promising cycling performance and a high capacity of 700 mAh g^{-1} after 100 cycles. By increasing the WN cathode loading to 9.5 and 12.5 mg cm^{-2}, an improved capacity of 980 and 1283 mAh g^{-1} after 100 cycles was observed. The superior performance of WN was attributed to the existence of S–WN bonding at the electrode surface, which indicated a strong interaction between lithium polysulfides and WN. Although these results indicated that WN was a highly

Encyclopedia of Inorganic and Bioinorganic Chemistry, Online © 2011–2019 John Wiley & Sons, Ltd.

This article was published in the *Encyclopedia of Inorganic and Bioinorganic Chemistry* in 2019 by John Wiley & Sons, Ltd.
DOI: 10.1002/9781119951438.eibc2687

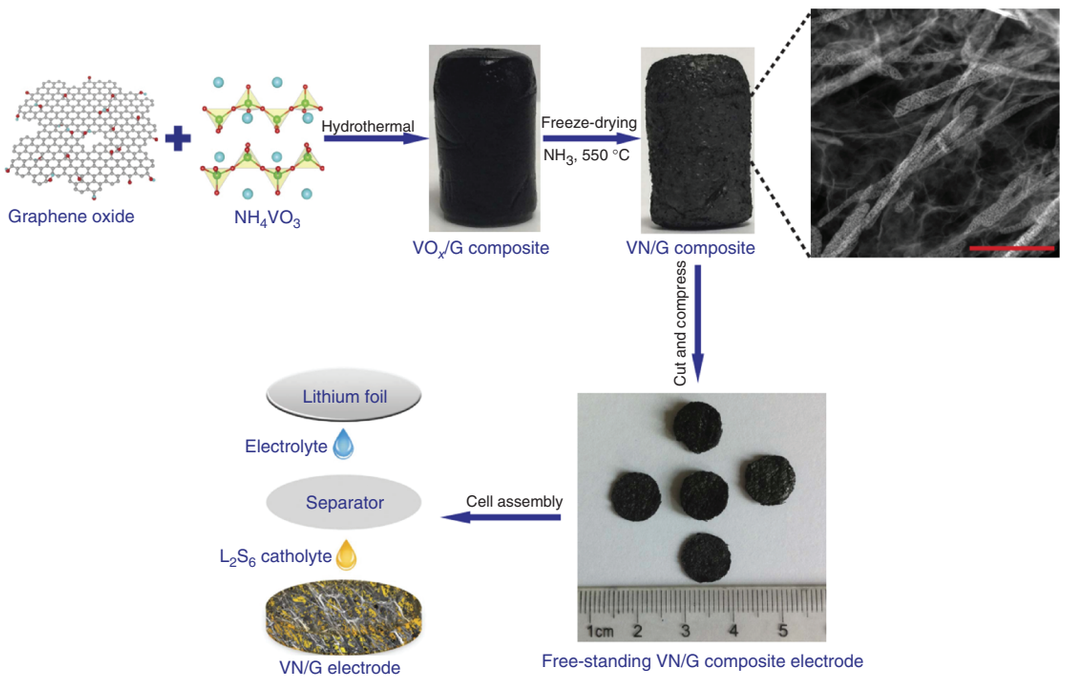

Figure 19 Schematic of the fabrication of a porous VN/G composite and the cell assembly with corresponding optical images of the material obtained. Scale bar 500 nm. [Reprinted with permission from Ref. 88. © Nature Publishing Group, 2017]

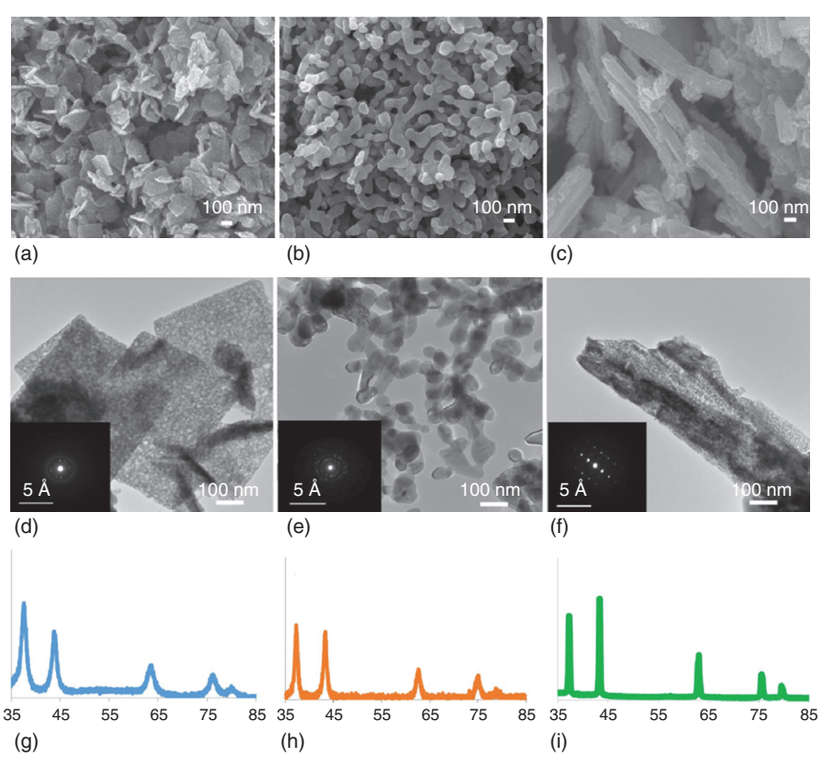

Figure 20 SEM image of (a) WN, (b) VN, and (c) Mo_2N. TEM images and SAED patterns of (d) WN, (e) VN, and (f) Mo_2N. Powder XRD patterns of (g) WN, (h) VN, and (i) Mo_2N. [Reprinted with permission from Ref. 90. © Elsevier, 2017]

Encyclopedia of Inorganic and Bioinorganic Chemistry, Online © 2011–2019 John Wiley & Sons, Ltd.

This article was published in the *Encyclopedia of Inorganic and Bioinorganic Chemistry* in 2019 by John Wiley & Sons, Ltd.
DOI: 10.1002/9781119951438.eibc2687

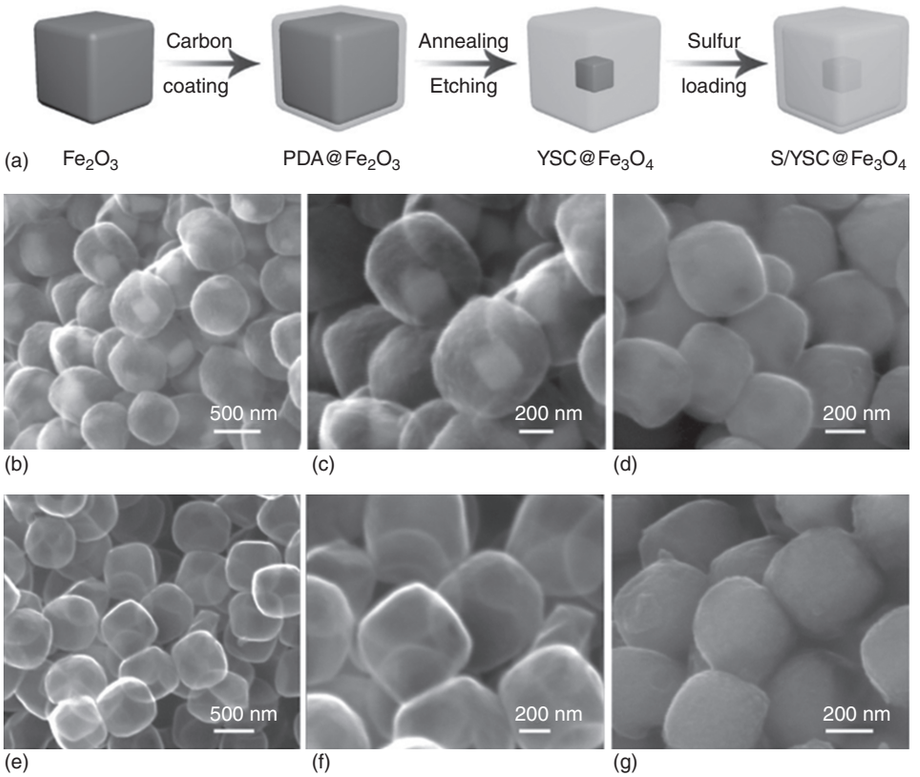

Figure 21 (a) Schematic of the synthetic procedure of the S/YSC@Fe_3O_4 composite. SEM images of (b,c) YSC@Fe_3O_4, (d) S/YSC@Fe_3O_4, (e,f) C nanobox, and (g) S/C nanobox. [Reprinted with permission from Ref. 91. © Wiley-VCH Verlag GmbH & Co. KGaA, 2017]

promising candidate for high-performance Li–S batteries, delicate structure modification was required to further improve its cycling stability.

2.3.4 Transition Metal Oxides

Recently, He *et al.*[91] reported the preparation of well-defined yolk-shell-like carbon@Fe_3O_4 (YSC@Fe_3O_4) nanoboxes and their utilization as sulfur hosts for Li–S batteries (Figure 21). Thanks to both physical confinement of carbon shells and strong chemical interaction with Fe_3O_4 cores, this unique nanoarchitecture effectively immobilized the active material and inhibited diffusion of polysulfide intermediate species. Moreover, due to their high conductivity, the carbon shells and the polar Fe_3O_4 cores facilitated fast electron/ion transport and promoted continuous reactivation of the active material during the charge/discharge process, resulting in improved electrochemical utilization and reversibility. The resulting S/YSC@Fe_3O_4 cathode, at a sulfur loading of 2.2 mg cm^{-2}, delivered a high initial specific capacity of 1366 mAh g^{-1}. After 200 cycles, the capacity was still stabilized at 1165 mAh g^{-1}, corresponding to a high capacity retention of 85.3% and a capacity fading rate of only 0.07% per cycle. For a comparison, the S/C nanobox-based cathode suffered from a severe capacity fade with a low capacity of 532 mAh g^{-1} after 200 cycles. These results clearly demonstrate that polysulfide dissolution was effectively mitigated in the S/YSC@Fe_3O_4 cathode.

In another study, Liu *et al.*[92] constructed a multifunctional interlayer on a separator by depositing Fe_3O_4 nanoparticles on a porous graphene film to immobilize polysulfides via strong chemical interaction (Figure 22). The graphene layer acted as a physical barrier of polysulfides and guaranteed good Li-ion transport, whereas Fe_3O_4 nanoparticles were able to chemically immobilize polysulfides. After optimizing the interlayer, the Li–S batteries showed an excellent cycling performance (732 mAh g^{-1} after 500 cycles and 356 mAh g^{-1} after total 2000 cycles at 1 C with a 49.0% capacity retention and capacity decay rate of 0.02%) and a superior rate capability (589 mAh g^{-1} at 2 C and 1423 mAh g^{-1} at 0.1 C).

In addition, a previous report demonstrated that coating a common S–C cathode with a thin layer of mesoporous TiO_2 promoted the interaction between TiO_2 and S, which was believed to be an electrostatic attraction (S–Ti–O)[93] and hence improved the adsorption of lithium polysulfides on TiO_2 surface. Similarly, Xiao *et al.*[94] prepared an

Encyclopedia of Inorganic and Bioinorganic Chemistry, Online © 2011–2019 John Wiley & Sons, Ltd.

This article was published in the *Encyclopedia of Inorganic and Bioinorganic Chemistry* in 2019 by John Wiley & Sons, Ltd.
DOI: 10.1002/9781119951438.eibc2687

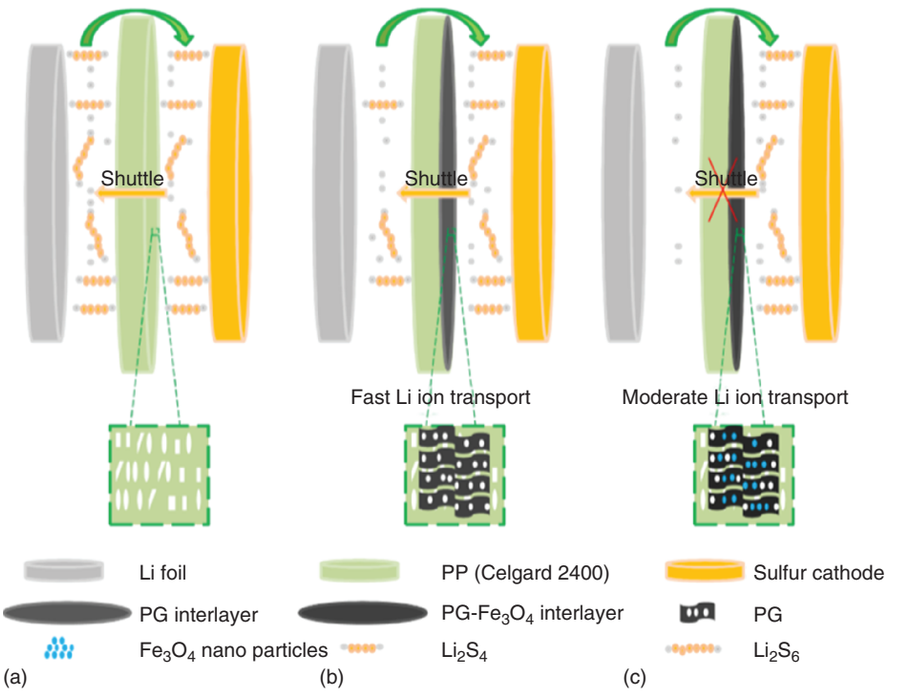

Figure 22 Schematic configuration of Li–S batteries with (a) a PP (polypropylene, Celgard 2400) separator; (b) porous graphene (PG)@PP; and (c) PG-Fe_3O_4@ PP interlayer. [Reprinted with permission from Liu, Y.; Qin, X.; Zhang, S.; Liang, G.; Kang, F.; Chen, G.; Li, B. Fe_3O_4-decorated porous graphene interlayer for high-performance lithium-sulfur batteries. ACS applied materials & interfaces 2018. © 2018, American Chemical Society]

integrated selective interlayer simply by coating the surface of a C–S cathode with a commercial graphene/TiO_2 film, which accounted for only ca. 7.8 wt% of the whole cathode. In this composite cathode, the porous graphene afforded an additional electrically conductive network, and physically trapped S and the intermediate lithium polysulfides; while TiO_2 in the graphene/TiO_2 barrier film further chemically suppressed the dissolution of lithium polysulfides, and hence greatly alleviated the undesirable shuttle effect. The thus-prepared cathode coated with a graphene/TiO_2 film was able to deliver a reversible specific capacity of ca. 1040 mAh g^{-1} over 300 cycles at 0.5 C. Ultralow capacity decay rates of 0.01 and 0.018% per cycle were observed at 2 and 3 C, respectively, over 1000 cycles.

Luo *et al.*[95] reported a novel strategy for decorating the separator with an interwoven MoO_3@CNT scaffold as an interlayer for trapping polysulfides in Li–S batteries (Figure 23). The conductive CNT networks facilitated electron transport, resulting in high rate capabilities. The polar MoO_3 nanorods tightly enfolded by CNTs (Figure 24) provided potent chemical interaction with polysulfides, thus mitigating the shuttle effect and giving rise to a longer cycle life. Moreover, such a dense coating of MoO_3@CNTs but with a porous structure also reserved abundant ion transfer channels. Therefore, the thin MoO_3@CNT hybrid interlayer could immobilize polysulfides without sacrificing fast lithium-ion transport. As a result, the Li–S batteries with the MoO_3@CNT interlayer showed remarkable electrochemical performances, with specific capacities of 1251 and 655 mAh g^{-1} at 0.3 C and 3 C, respectively. After 200 cycles at 0.3 C, the batteries still retained a high capacity of 755 mAh g^{-1}. Furthermore, the facilely synthesized MoO_3@CNT hybrid layer was also able to buffer the large volume fluctuation of sulfur cathode during cycling process.

2.3.5 *Transition Metal Carbides*

Metal carbides as a cathode material for Li–S battery have been widely studied since the discovery of Ti_3C_2 in 2011. Compared to other metal compounds such as sulfide, oxide, and phosphide, carbides have many unique characteristics: (i) high electrical conductivity; (ii) excellent chemical and physical stability; and (iii) high electrocatalytic activity for the redox processes of lithium polysulfides. In 2015, Nazar and coworkers[96] first reported a new class of sulfur host materials the so-called delaminated MXene phases that capitalized on a combination of inherently high conductivity and highly active 2D surfaces to chemically bond intermediate polysulfides by metal–sulfur interactions, providing a very stable cycling performance and high capacity even at 70 wt% S. With the

Encyclopedia of Inorganic and Bioinorganic Chemistry, Online © 2011–2019 John Wiley & Sons, Ltd.

This article was published in the *Encyclopedia of Inorganic and Bioinorganic Chemistry* in 2019 by John Wiley & Sons, Ltd.
DOI: 10.1002/9781119951438.eibc2687

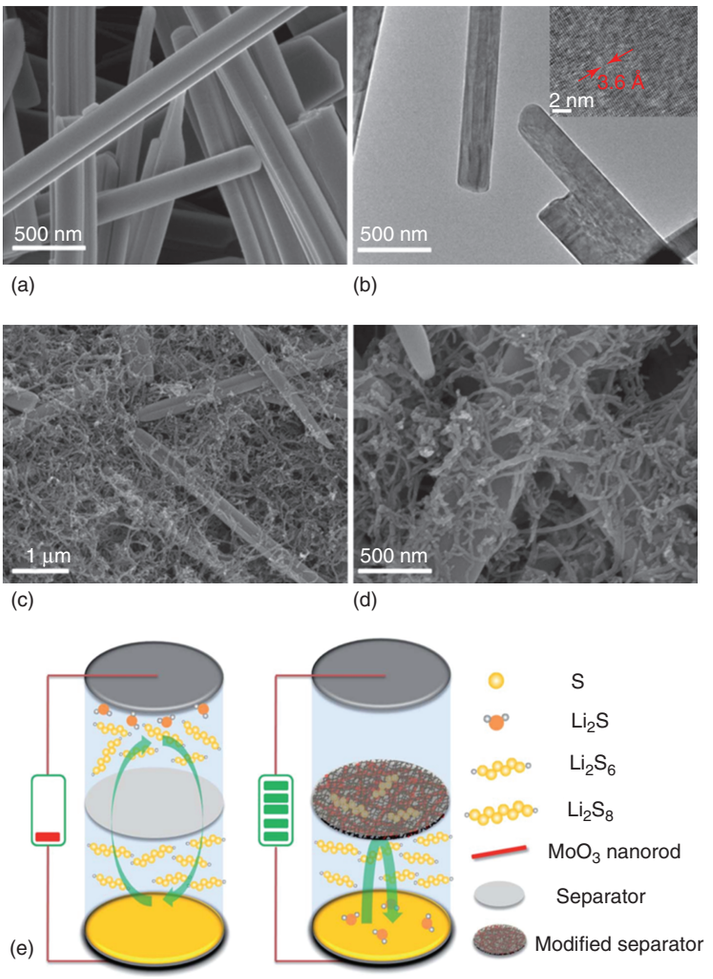

Figure 23 (a) SEM and (b) TEM images of MoO_3 nanorods; (c–d) SEM images of the interwoven MoO_3@CNT framework. (e) Schematic of Li–S batteries with original and MoO_3@CNT modified separators. [Reprinted with permission from Ref. 95. © Royal Society of Chemistry, 2018]

aid of XPS analysis, the authors verified that sulfur/sulfide species replaced the hydroxy groups on Ti_2C surface, forming a strong Ti–S interaction with the core, as shown in Figure 24. Specifically, the optimized 70S/d-Ti_2C-based cathode delivered a discharge capacity of 1090 mAh g^{-1} at a 0.5 C rate (837 mA g^{-1}) and while at 1 C (1675 mA g^{-1}) the discharge capacity was still as high as1000 mAh g^{-1} and showed excellent cycling stability at various rates in Figure 24(b)–(d).

Among the metal carbides discovered to date, niobium carbide (NbC) delivers the highest electrical conductivity up to 2.9×10^6 S m^{-1} and excellent mechanical and chemical stabilities, while its polar molecular structure offers strong chemical interactions with polysulfide anions. Hence NbC can serve as a potential interlayer material for Li–S batteries. Zhu and coworkers[97] reported a facile autoclave method to synthesize nanocrystalline NbC through a magnesiothermic reaction at 600 °C, as shown in Figure 25, and the sulfur cathode employing the NbC-coated membrane exhibited outstanding cyclability over 1500 cycles, excellent rate capability up to 5 C, and high areal capacity of 3.6 mAh cm^{-2} with a relatively high sulfur loading of 4 mg cm^{-2} in a coin cell, as well as a reliable operation in soft package.

In a recent study, Wang *et al.*[98] infiltrated unexfoliated Ti_3C_2 stacks with molten sulfur, which was then coated with a thin layer of porous polydopamine. The electrically conductive MXene sheets, that is, Ti_3C_2, contained a number of Lewis-acid Ti-sites which enabled the Lewis acid–base interaction with Li_2S_x. At the same time, the polar N- and O-atom in the polydopamine layer bound strongly with polar Li^+, further immobilizing Li_2S_x within the cathode. Such a combined Li_2S_x immobilization effect offered by the MXene matrix and polydopamine layer

Encyclopedia of Inorganic and Bioinorganic Chemistry, Online © 2011–2019 John Wiley & Sons, Ltd.

This article was published in the *Encyclopedia of Inorganic and Bioinorganic Chemistry* in 2019 by John Wiley & Sons, Ltd.
DOI: 10.1002/9781119951438.eibc2687

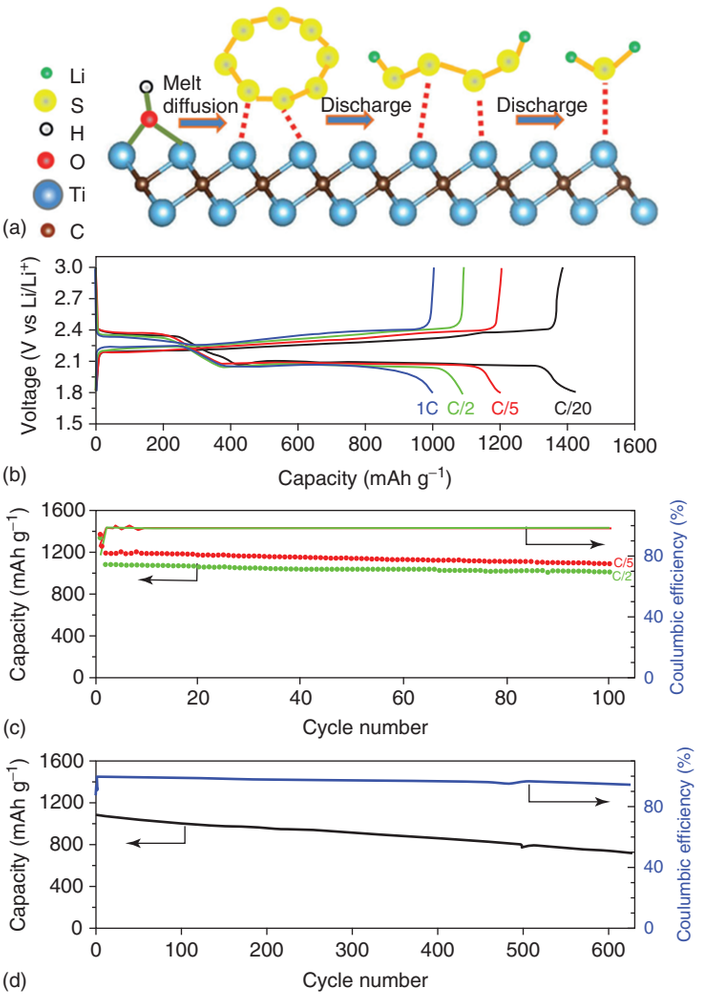

Figure 24 (a) Replacement of the Ti—OH bond on the MXene surface with a S—Ti—C bond by heat treatment or by contact with polysulfides. (b) Voltage profiles of 70S/d-Ti_2C at various rates ranging from 0.05 to 1 C. (c) Cycling performance of 70S/d-Ti_2C at 0.2 and 0.5 C. (d) Long-term cycling at 0.5 C. Cells are conditioned for the first cycle at 0.05 C to facilitate electrode wetting. The increase in rate on the 2nd cycle results in a change in capacity. [Reprinted with permission from Ref. 96. Wiley-VCH Verlag GmbH & Co. KGaA, 2015]

helped maximize the Li_2S_x immobilization and allowed the new S-cathodes to exhibit high and stable energy/rate capacity even at a high S loading. Specifically, the capacity decay was only 0.035% per cycle, which was achieved at a sulfur loading of 5 mg cm^{-2}. Meanwhile, the electrode kinetics of cathode with a high sulfur loading was also promoted by the efficient deposition of Li_2S driven by the dual Li_2S_x immobilization and the conductive network stabilized by polydopamine.[20,98,99]

3 SUMMARY AND OUTLOOK

Dissolution of intermediate lithium polysulfides from cathode to organic electrolyte and their subsequent diffusion toward the anode are two main reasons for rapid capacity degradation, low Coulombic efficiency, and poor sulfur utilization. A number of methods, such as physical confinement, covalent bonding to form polymeric sulfur, and incorporation of polar anchoring materials, have been developed for cathode engineering to effectively mitigate or even suppress these two processes, so as to maximize the potential of Li–S battery and realize its high capacity and energy density, as compared to traditional lithium-ion batteries. An ideal material for shielding polysulfide dissolution and diffusion should have sufficiently strong bonding/binding interactions with the Li_2S_x species, high electron and ion conductivity, good catalytic activity for the polysulfides redox process as well as light-weight, low cost, high electrochemical and mechanical stability. In addition,

Encyclopedia of Inorganic and Bioinorganic Chemistry, Online © 2011–2019 John Wiley & Sons, Ltd.

This article was published in the *Encyclopedia of Inorganic and Bioinorganic Chemistry* in 2019 by John Wiley & Sons, Ltd.
DOI: 10.1002/9781119951438.eibc2687

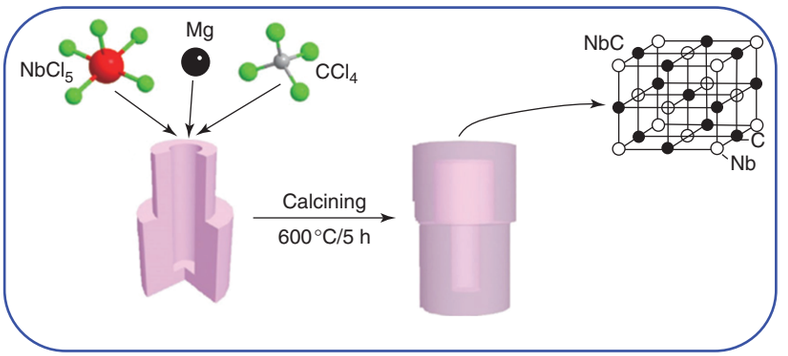

Figure 25 Schematic illustration of the preparation of NbC. Many other carbides have been used as host materials for Li–S batteries, such as MoC and Wo_2C. For examples, Yu's group prepared MoC nanoparticles encapsulated in N-doped carbon nanofibers (NCF), theoretical calculations, adsorption experiments, and cyclic voltammetry analysis proved that MoC is active sites on the electrode with double functionality: to improve both the cycling stability and rate capability of Li–S batteries via the dual effect of providing adsorption and catalytic sites. [Reprinted with permission from Ref. 97. Wiley-VCH Verlag GmbH & Co. KGaA, 2018]

the traditional composite materials based on an active sulfur yolk and a conductive shell having strong binding strength toward polysulfides, as well as the vast family of metal–organic framework hosts[100] will demonstrate high potential in the preparation of efficient polysulfides immobilizers for long-life sulfur cathodes.[101–103] These will be the foci of future research.

4 ACKNOWLEDGMENTS

This work was supported by the National Natural Science Foundation of China (NSFC Grant No. 21528301 and 51402111), and the Fundamental Research Funds for the Central Universities (SCUT Grant No. 201522/05).

5 RELATED ARTICLES

Li-Ion Batteries and Beyond: Future Design Challenges; Lithium–Ion Batteries; Sulfur: Organic Polysulfanes; Sulfur: Inorganic Chemistry

6 REFERENCES

1. H. Danuta, U. Juliusz, Electric Dry Cells and Storage Batteries, US, Patent 3,043,896[P], 1962-7-10.
2. Y. Yang, G. Zheng and Y. Cui, *Chem. Soc. Rev.*, 2013, **42**, 3018.
3. J. Song, M. L. Gordin, T. Xu, S. Chen, Z. Yu, H. Sohn, J. Lu, Y. Ren, Y. Duan and D. Wang, *Angew. Chem.*, 2015, **127**, 4399.
4. M. A. Pope and I. A. Aksay, *Adv. Energy Mater.*, 2015, **5**, 1500124.
5. B. Ji, F. Zhang, M. Sheng, X. Tong and Y. Tang, *Adv. Mater.*, 2017, **29**, 1604219.
6. C.-X. Zu and H. Li, *Energy Environ. Sci.*, 2011, **4**, 2614.
7. H. S. Kang and Y. K. Sun, *Adv. Funct. Mater.*, 2016, **26**, 1225.
8. X. Gu, C.-j. Tong, C. Lai, J. Qiu, X. Huang, W. Yang, B. Wen, L.-m. Liu, Y. Hou and S. Zhang, *J. Mater. Chem. A*, 2015, **3**, 16670.
9. L. Borchardt, M. Oschatz and S. Kaskel, *Chem. Eur. J.*, 2016, **22**, 7324.
10. W. J. Chung, J. J. Griebel, E. T. Kim, H. Yoon, A. G. Simmonds, H. J. Ji, P. T. Dirlam, R. S. Glass, J. J. Wie and N. A. Nguyen, *Nat. Chem.*, 2013, **5**, 518.
11. V. Etacheri, R. Marom, R. Elazari, G. Salitra and D. Aurbach, *Energy Environ. Sci.*, 2011, **4**, 3243.
12. N. Osada, C. B. Bucur, H. Aso and J. Muldoon, *Energy Environ. Sci.*, 2016, **9**, 1668.
13. Y. Xiang, J. Li, J. Lei, D. Liu, Z. Xie, D. Qu, K. Li, T. Deng and H. Tang, *ChemSusChem*, 2016, **9**, 3023.
14. J. Wang, Y. S. He and J. Yang, *Adv. Mater.*, 2015, **27**, 569.
15. H. Wang, W. Zhang, H. Liu and Z. Guo, *Angew. Chem. Int. Ed.*, 2016, **55**, 3992.
16. H. Cheng and S. Wang, *J. Mater. Chem. A*, 2014, **2**, 13783.
17. X. Ji and L. F. Nazar, *J. Mater. Chem.*, 2010, **20**, 9821.
18. G. C. Li, G. R. Li, S. H. Ye and X. P. Gao, *Adv. Energy Mater.*, 2012, **2**, 1238.
19. F. Wu, J. Qian, R. Chen, T. Zhao, R. Xu, Y. Ye, W. Li, L. Li, J. Lu and K. Amine, *Nano Energy*, 2015, **12**, 742.
20. A. Rosenman, E. Markevich, G. Salitra, D. Aurbach, A. Garsuch and F. F. Chesneau, *Adv. Energy Mater.*, 2015, **5**, 1500212.

DOI: 10.1002/9781119951438.eibc2687

21. Z. Li, Y. Huang, L. Yuan, Z. Hao and Y. Huang, *Carbon*, 2015, **92**, 41.
22. G. Li, J. Sun, W. Hou, S. Jiang, Y. Huang and J. Geng, *Nat. Commun.*, 2016, **7**, 10601.
23. M. Yan, Y. Zhang, Y. Li, Y. Huo, Y. Yu, C. Wang, J. Jin, L. Chen, T. Hasan and B. Wang, *J. Mater. Chem. A*, 2016, **4**, 9403.
24. N. A. Lange ed., 'Lange's Handbook of Chemistry', McGraw-Hill Education, 2016.
25. E. Peled, A. Gorenshtein, M. Segal and Y. Sternberg, *J. Power Sources*, 1989, **26**, 269.
26. X. Ji, K. T. Lee and L. F. Nazar, *Nat. Mater.*, 2009, **8**, 500.
27. A. Manthiram, Y. Fu and Y. S. Su, *Acc. Chem. Res.*, 2013, **46**, 1125.
28. N. Jayaprakash, J. Shen, S. S. Moganty, A. Corona and L. A. Archer, *Angew. Chem. Int. Ed.*, 2011, **50**, 5904.
29. G. Buechel, K. K. Unger, A. Matsumoto and K. Tsutsumi, *Adv. Mater.*, 1999, **10**, 1036.
30. F. Xu, Z. Tang, S. Huang, L. Chen, Y. Liang, W. Mai, H. Zhong, R. Fu and D. Wu, *Nat. Commun.*, 2015, **6**, 7221.
31. W. Zhou, Y. Yu, H. Chen, F. J. Disalvo and H. D. Abruña, *J. Am. Chem. Soc.*, 2013, **135**, 16736.
32. R. H. Baughman, A. A. Zakhidov and W. A. D. Heer, *Science*, 2002, **297**, 787.
33. R. B. Heimann, S. E. Evsvukov and Y. Koga, *Carbon*, 1997, **35**, 1654.
34. P. Morgan, Carbon Fibers and Their Composites, Marcel Dekker, 2005.
35. K. Shirvanimoghaddam, S. U. Hamim, M. K. Akbari, S. M. Fakhrhoseini, H. Khayyam, A. H. Pakseresht, E. Ghassali, M. Zabet, K. S. Munir and S. Jia, *Compos. A Appl. Sci. Manuf.*, 2017, **92**, 70.
36. Y. Zhao, W. Wu, J. Li, Z. Xu and L. Guan, *Adv. Mater.*, 2014, **26**, 5113.
37. D. W. Wang, Q. Zeng, G. Zhou, L. Yin, F. Li, H. M. Cheng, I. R. Gentle and G. Q. M. Lu, *J. Mater. Chem. A*, 2013, **1**, 9382.
38. J. Guo, Y. Xu and C. Wang, *Nano Lett.*, 2011, **11**, 4288.
39. S. Xin, L. Gu, N. H. Zhao, Y. X. Yin, L. J. Zhou, Y. G. Guo and L. J. Wan, *J. Am. Chem. Soc.*, 2012, **134**, 18510.
40. G. Zheng, Y. Yang, J. J. Cha, S. S. Hong and Y. Cui, *Nano Lett.*, 2011, **11**, 4462.
41. K. S. Novoselov, A. K. Geim, S. V. Morozov, D. Jiang, Y. Zhang, S. V. Dubonos, I. V. Grigorieva and A. A. Firsov, *Science*, 2004, **306**, 666.
42. H. Wang, H. S. Casalongue, Y. Liang and H. Dai, *J. Am. Chem. Soc.*, 2010, **132**, 7472.
43. H. Wang, Y. Yang, Y. Liang, J. T. Robinson, Y. Li, A. Jackson, Y. Cui and H. Dai, *Nano Lett.*, 2011, **11**, 2644.
44. Y. Qiu, W. Li, W. Zhao, G. Li, Y. Hou, M. Liu, L. Zhou, F. Ye, H. Li, Z. Wei, S. Yang, W. Duan, Y. Ye, J. Guo and Y. Zhang, *Nano Lett.*, 2014, **14**, 4821.
45. C. Zhang, W. Lv, W. Zhang, X. Zheng, M. B. Wu, W. Wei, Y. Tao, Z. Li and Q. H. Yang, *Adv. Energy Mater.*, 2013, **4**, 1301565.
46. M. Q. Zhao, Q. Zhang, J. Q. Huang, G. L. Tian, J. Q. Nie, H. J. Peng and F. Wei, *Nat. Commun.*, 2014, **5**, 3410.
47. L. Hu, J. W. Choi, Y. Yang, S. Jeong, F. La Mantia, L.-F. Cui and Y. Cui, *Proc. Natl. Acad. Sci.*, 2009, **106**, 21490.
48. G. Zhou, S. Pei, L. Li, D. W. Wang, S. Wang, K. Huang, L. C. Yin, F. Li and H. M. Cheng, *Adv. Mater.*, 2014, **26**, 625.
49. D.-W. Wang, F. Li, M. Liu, G. Q. Lu and H.-M. Cheng, *Angew. Chem. Int. Ed.*, 2008, **47**, 373.
50. Z. M. Zheng, H. C. Guo, F. Pei, X. Zhang, X. Y. Chen, X. L. Fang, T. H. Wang and N. F. Zheng, *Adv. Funct. Mater.*, 2016, **26**, 8952.
51. C. Hoffmann, S. Thieme, J. Brückner, M. Oschatz, T. Biemelt, G. Mondin, H. Althues and S. Kaskel, *ACS Nano*, 2014, **8**, 12130.
52. Z. Yuan, H.-J. Peng, J.-Q. Huang, X.-Y. Liu, D.-W. Wang, X.-B. Cheng and Q. Zhang, *Adv. Funct. Mater.*, 2014, **24**, 6105.
53. Z. Li, L. X. Yuan, Z. Q. Yi, Y. M. Sun, Y. Liu, Y. Jiang, Y. Shen, Y. Xin, Z. L. Zhang and Y. H. Huang, *Adv. Energy Mater.*, 2014, **4**, 1301473.
54. G. Hu, Z. Sun, C. Shi, R. Fang, J. Chen, P. Hou, C. Liu, H. M. Cheng and F. Li, *Adv. Mater.*, 2017, **29**, 1603835.
55. S. Zeng, L. Li, J. Yu, N. Wang and S. Chen, *Electrochim. Acta*, 2018, **263**, 53.
56. B. Oschmann, J. Park, C. Kim, K. Char, Y.-E. Sung and R. Zentel, *Chem. Mater.*, 2015, **27**, 7011.
57. C. Fu, G. Li, J. Zhang, B. Cornejo, S. S. Piao, K. N. Bozhilov, R. C. Haddon and J. Guo, *ACS Energy Lett.*, 2016, **1**, 115.
58. J. Liu, M. Wang, N. Xu, T. Qian and C. Yan, *Energy Storage Mater.*, 2018, **15**, 53.
59. H. Kim, J. Lee, H. Ahn, O. Kim and M. J. Park, *Nat. Commun.*, 2015, **6**, 7278.
60. S.-Z. Zeng, Y. Yao, X. Zeng, Q. He, X. Zheng, S. Chen, W. Tu and J. Zou, *J. Power Sources*, 2017, **357**, 11.
61. S. Zeng, L. Li, L. Xie, D. Zhao, N. Zhou, N. Wang and S. Chen, *Carbon*, 2017, **122**, 106.
62. S. H. Je, T. H. Hwang, S. N. Talapaneni, O. Buyukcakir, H. J. Kim, J.-S. Yu, S.-G. Woo, M. C. Jang, B. K. Son and A. Coskun, *ACS Energy Lett.*, 2016, **1**, 566.
63. S. Zeng, L. Li, L. Xie, D. Zhao, N. Wang and S. Chen, *ChemSusChem*, 2017, **10**, 3378.
64. J. Wang, J. Yang, C. Wan, K. Du, J. Xie and N. Xu, *Adv. Funct. Mater.*, 2003, **13**, 487.
65. X.-g. Yu, J.-y. Xie, J. Yang, H.-j. Huang, K. Wang and Z.-s. Wen, *J. Electroanal. Chem.*, 2004, **573**, 121.
66. J. Fanous, M. Wegner, J. Grimminger, A. n. Andresen and M. R. Buchmeiser, *Chem. Mater.*, 2011, **23**, 5024.

Encyclopedia of Inorganic and Bioinorganic Chemistry, Online © 2011–2019 John Wiley & Sons, Ltd.

This article was published in the *Encyclopedia of Inorganic and Bioinorganic Chemistry* in 2019 by John Wiley & Sons, Ltd.
DOI: 10.1002/9781119951438.eibc2687

67. S. S. Zhang, *Energies*, 2014, **7**, 4588.
68. Y. Liu, A. K. Haridas, K.-K. Cho, Y. Lee and J.-H. Ahn, *J. Phys. Chem. C*, 2017, **121**, 26172.
69. S. N. Talapaneni, T. H. Hwang, S. H. Je, O. Buyukcakir, J. W. Choi and A. Coskun, *Angew. Chem. Int. Ed.*, 2016, **55**, 3106.
70. F. Xu, S. Yang, G. Jiang, Q. Ye, B. Wei and H. Wang, *ACS Appl. Mater. Interfaces*, 2017, **9**, 37731.
71. Q. Zhang, Y. Wang, Z. W. Seh, Z. Fu, R. Zhang and Y. Cui, *Nano Lett.*, 2015, **15**, 3780.
72. T. Z. Hou, X. Chen, H. J. Peng, J. Q. Huang, B. Q. Li, Q. Zhang and B. Li, *Small*, 2016, **12**, 3283.
73. Q. Pang, J. Tang, H. Huang, X. Liang, C. Hart, K. C. Tam and L. F. Nazar, *Adv. Mater.*, 2015, **27**, 6021.
74. Q. Pang and L. F. Nazar, *ACS Nano*, 2016, **10**, 4111.
75. X. Liu, J. Q. Huang, Q. Zhang and L. Mai, *Adv. Mater.*, 2017, **29**, 1601759.
76. X. Y. Yu, L. Yu and X. W. Lou, *Adv. Energy Mater.*, 2016, **6**, 1501333.
77. L. Ma, S. Wei, H. L. Zhuang, K. E. Hendrickson, R. G. Hennig and L. A. Archer, *J. Mater. Chem. A*, 2015, **3**, 19857.
78. L. Ma, H. Zhuang, Y. Lu, S. S. Moganty, R. G. Hennig and L. A. Archer, *Adv. Energy Mater.*, 2014, **4**, 1400390.
79. Z. W. Seh, J. H. Yu, W. Li, P.-C. Hsu, H. Wang, Y. Sun, H. Yao, Q. Zhang and Y. Cui, *Nat. Commun.*, 2014, **5**, 5017.
80. G. Zhou, H. Tian, Y. Jin, X. Tao, B. Liu, R. Zhang, Z. W. Seh, D. Zhuo, Y. Liu and J. Sun, *Proc. Natl. Acad. Sci.*, 2017, **114**, 840.
81. M. Q. Zhao, X. F. Liu, Q. Zhang, G. L. Tian, J. Q. Huang, W. Zhu and F. Wei, *ACS Nano*, 2012, **6**, 10759.
82. R. E. Jones, F. S. Gittleson, J. A. Templeton and D. K. Ward, *J. Electrochem. Soc.*, 2017, **164**, A6422.
83. X. Tao, J. Wang, C. Liu, H. Wang, H. Yao, G. Zheng, Z. W. Seh, Q. Cai, W. Li and G. Zhou, *Nat. Commun.*, 2016, **7**, 11203.
84. M. S. Faber, R. Dziedzic, M. A. Lukowski, N. S. Kaiser, Q. Ding and S. Jin, *J. Am. Chem. Soc.*, 2014, **136**, 10053.
85. Z. Yuan, H. J. Peng, T. Z. Hou, J. Q. Huang, C. M. Chen, D. W. Wang, X. B. Cheng, F. Wei and Q. Zhang, *Nano Lett.*, 2016, **16**, 519.
86. S. Rehman, S. Guo and Y. Hou, *Adv. Mater.*, 2016, **28**, 3167.
87. Q. Pang, D. Kundu and L. F. Nazar, *Mater. Horiz.*, 2016, **3**, 130.
88. Z. Sun, J. Zhang, L. Yin, G. Hu, R. Fang, H.-M. Cheng and F. Li, *Nat. Commun.*, 2017, **8**, 14627.
89. Z. Cui, C. Zu, W. Zhou, A. Manthiram and J. B. Goodenough, *Adv. Mater.*, 2016, **28**, 6926.
90. N. Mosavati, S. O. Salley and K. S. Ng, *J. Power Sources*, 2017, **340**, 210.
91. J. He, L. Luo, Y. Chen and A. Manthiram, *Adv. Mater.*, 2017, **29**, 1702707.
92. Y. Liu, X. Qin, S. Zhang, G. Liang, F. Kang, G. Chen and B. Li, *ACS Appl. Mater. Interfaces*, 2018, **10**, 26264.
93. Z. Liang, G. Zheng, W. Li, Z. W. Seh, H. Yao, K. Yan, D. Kong and Y. Cui, *ACS Nano*, 2014, **8**, 5249.
94. Z. Xiao, Z. Yang, L. Wang, H. Nie, M. Zhong, Q. Lai, X. Xu, L. Zhang and S. Huang, *Adv. Mater.*, 2015, **27**, 2891.
95. L. Luo, X. Qin, J. Wu, G. Liang, Q. Li, M. Liu, F. Kang, G. Chen and B. Li, *J. Mater. Chem. A*, 2018, **6**, 8612.
96. X. Liang, A. Garsuch and L. F. Nazar, *Angew. Chem.*, 2015, **127**, 3979.
97. W. Cai, G. Li, K. Zhang, G. Xiao, C. Wang, K. Ye, Z. Chen, Y. Zhu and Y. Qian, *Adv. Funct. Mater.*, 2018, **28**, 1704865.
98. X. Wang, C. Yang, X. Xiong, G. Chen, M. Huang, J.-H. Wang, Y. Liu, M. Liu and K. Huang, *Energy Storage Mater.*, 2019, **16**, 344.
99. A. Manthiram, Y. Fu, S.-H. Chung, C. Zu and Y.-S. Su, *Chem. Rev.*, 2014, **114**, 11751.
100. H. Jiang, X. C. Liu, Y. Wu, Y. Shu, X. Gong, F. S. Ke and H. Deng, *Angew. Chem.*, 2018, **130**, 3980.
101. Z. W. Seh, W. Li, J. J. Cha, G. Zheng, Y. Yang, M. T. McDowell, P.-C. Hsu and Y. Cui, *Nat. Commun.*, 2013, **4**, 1331.
102. A. S. Arico, P. Bruce, B. Scrosati, J.-M. Tarascon and W. V. Schalkwijk, in 'Materials For Sustainable Energy: A Collection of Peer-Reviewed Research and Review Articles from Nature Publishing Group', ed. W. Van Schalkwijk, World Scientific, 2011, p.148.
103. Y. G. Guo, J. S. Hu and L. J. Wan, *Adv. Mater.*, 2008, **20**, 2878.

Encyclopedia of Inorganic and Bioinorganic Chemistry, Online © 2011–2019 John Wiley & Sons, Ltd.

This article was published in the *Encyclopedia of Inorganic and Bioinorganic Chemistry* in 2019 by John Wiley & Sons, Ltd.
DOI: 10.1002/9781119951438.eibc2687